Energetically consistent Eddy-Diffusivity Mass-Flux schemes. Part II: implementation and evaluation in an oceanic context.

Manolis Perrot, Florian Lemarié

Energetically consistent Eddy-Diffusivity Mass-Flux convective schemes. Part II: Implementation and Evaluation in an oceanic context.

M. Perrot[1,*], **F. Lemarié**[1]

[1]Univ. Grenoble Alpes, Inria, CNRS, Grenoble INP, LJK, Grenoble, France

Key Points:

- The assumptions underlying the derivation of Mass Flux (MF) schemes are evaluated in the oceanic context using scaling analysis and LES simulations
- Based on LES results, a new closure for the turbulent transport of Turbulent Kinetic Energy (TKE) taking into account MF transport of TKE is proposed
- Guided by continuous energy budgets, an energy-conserving discretization is proposed, and energy biases of inconsistent formulations are quantified

Corresponding author: Manolis Perrot, `manolis.perrot@univ-grenoble-alpes.fr`

Abstract

A convective vertical mixing scheme rooted in the Eddy-Diffusivity Mass-Flux (EDMF) approach is carefully derived from first principles in Part I. In addition, consistent energy budgets between resolved and subgrid scales when using an EDMF scheme are presented for seawater and dry atmosphere. In this second part, we focus on oceanic convection with the following objectives in mind: (*i*) justify in the oceanic context the assumptions made in Part I for the derivation of an MF scheme and a new TKE turbulent transport term (*ii*) show how continuous energy budgets can guide an energetically-consistent discretization (*iii*) quantify energy biases of inconsistent formulations, including double-counting errors due to inconsistent boundary conditions. The performance of the proposed energetically consistent EDMF scheme is evaluated against Large Eddy Simulations (LES) and observational data of oceanic convection. We systematically evaluate the sensitivity of numerical solutions to different aspects of the new formulation we propose. Notably, when compared to LES data, energetic consistency is key to obtaining accurate TKE and turbulent transport of TKE profiles. To further illustrate that the MF concept is a credible alternative to the traditional approaches used in the oceanic context (using an enhanced vertical diffusion or a counter gradient term) the proposed scheme is validated in a single-column configuration against observational data of oceanic convection from the LION buoy.

Plain Language Summary

In Earth system models, various important processes occur on scales that are too fine to be resolved with usual grid resolutions. Parameterizations have to be used to approximate the average effect of such processes on the scales resolved by a numerical model. The general objective of the proposed work is to approach the parameterization problem for boundary-layer turbulence and convective plumes in a "consistent" manner. Here the notion of consistency integrates various aspects: global energetic consistency, consistency with a particular averaging technique for the scale-separation, and the rigorous reduction of a physical system to a scale-aware parametric representation based on well-identified and justifiable approximations and hypotheses. An originality is to jointly consider energy budgets including a subgrid energy reservoir on top of the resolved energies allowing the proper coupling between the parameterization and the resolved fluid dynamics. In the first part of this work, we focused on theoretical aspects at the continuous level. In this second part, we look at the practical aspects of implementing the proposed concepts in an oceanic numerical model. This research paves the way toward an alternative methodology to parameterize oceanic convection across scales. Numerical simulations demonstrate the adequacy of the proposed parameterization.

1 Introduction

Oceanic vertical mixing parameterizations based on the Eddy-Diffusivity Mass-Flux (EDMF) concept have seen a growing interest in the past years (Giordani et al., 2020; Garanaik et al., 2024; Ramadhan et al., 2020). In the companion paper Perrot et al. (2024) (hereafter Part I), we provide a self-contained derivation from first principles of a convective mixing EDMF scheme. This type of closure involves separating vertical turbulent fluxes into two components: an eddy-diffusivity (ED) term that addresses local small-scale mixing in a near isotropic environment, and a mass-flux (MF) transport term that accounts for the non-local transport performed by vertically coherent plumes within the environment. Using the multi-fluid averaging underlying the MF concept, we review consistent energy budgets between resolved and subgrid scales for seawater and dry atmosphere, in anelastic and Boussinesq settings. We show that when using an EDMF scheme, closed energy budgets can be recovered if: (*i*) bulk production terms of turbulent kinetic energy (TKE) by shear, buoyancy and transport include MF contributions; (*ii*) bound-

ary conditions are consistent with EDMF, to avoid spurious energy fluxes at the boundary. Moreover we show that lateral mixing between plumes and environment (referred as entrainment or detrainment) induces a net production of TKE via the shear term, and such production is enhanced when horizontal drag increases. Throughout the theoretical development of the scheme, we maintain transparency regarding underlying assumptions.

In this second part, we use Large Eddy Simulations of oceanic convection to: (*i*) evaluate the assumptions used in the derivation of the scheme using a conditional sampling of convective plumes, (*ii*) propose a new formulation for TKE transport and (*iii*) assess the sensitivity of the EDMF scheme to energetic consistency, transport of TKE, horizontal momentum transport and small plume area assumption. Additionally, we compare the scheme to the classical TKE+EVD mixing scheme used for oceanic deep-convection (Turbulent Kinetic Energy and Enhanced Vertical Diffusivity, Madec et al., 2019). We show how energy budgets derived in Part I can guide a consistent discretization of the TKE equation; and we quantify energy biases of inconsistent formulations, including double-counting errors due to inconsistent boundary conditions.

We consider a Single Column Model (SCM) of the ocean in Boussinesq approximation (e.g. Tailleux & Dubos, 2024),

$$\begin{cases} \partial_t \overline{\boldsymbol{u}}_h = -\partial_z \overline{w' \boldsymbol{u}'_h} \\ \partial_t \overline{\theta} = -\partial_z \overline{w'\theta'} + \frac{\overline{\epsilon}}{c_p - \alpha g z} \\ \partial_t \overline{S} = -\partial_z \overline{w' S'} \end{cases}$$

where $\overline{\boldsymbol{u}}_h = (\overline{u}, \overline{v})$ is the horizontal velocity vector, $\overline{\theta}$ is conservative temperature, $\overline{S}$ is salinity, and $\overline{w'\boldsymbol{u}'_h}$, $\overline{w'\theta'}$, $\overline{w'S'}$ are the corresponding vertical turbulent fluxes. Moreover $\overline{\epsilon}$ is the viscous dissipation of turbulence, c_p is the seawater specific heat capacity and α is the thermal expansion coefficient. The notation $\overline{(\cdot)}$ indicates that the model's variables and fluxes are interpreted as *horizontal averages* over the numerical grid cell of their continuous counterpart. Thus we have a simple and exact correspondence to compare SCM and LES data. Although viscous heating is usually neglected in the ocean (McDougall, 2003), we kept this term to obtain a closed energy budget.

The EDMF parameterization relies on a decomposition of the horizontal grid area into an isotropic environment where turbulence is assumed diffusive, and an averaged plume. Then the flux of any variable $X = u, v, \theta, S$ is closed according to the decomposition

$$\overline{w'X'} = \underbrace{-K_X \partial_z \overline{X}}_{\text{ED}} + \underbrace{a_p w_p (X_p - \overline{X})}_{\text{MF}} \tag{1}$$

where K_X is an eddy-diffusivity coefficient, a_p is the fractional area of the plume, w_p is the vertical velocity of the plume and X_p is the plume-related X quantity. In the present study, the eddy viscosity K_u and diffusivities $K_\phi = K_\theta = K_S$ in turbulent vertical fluxes are computed from a turbulence closure model based on a prognostic equation for the turbulent kinetic energy (TKE) $k = \overline{\boldsymbol{u}' \cdot \boldsymbol{u}'}/2$ and a diagnostic computation of appropriate length scales (a.k.a. 1.5-order turbulence closure, see Appendix A).

Total energy of the fluid in a Boussinesq approximation can be split into kinetic energy of the horizontal resolved flow $E_k = (\overline{\boldsymbol{u}}_h \cdot \overline{\boldsymbol{u}}_h)/2$ (usually referred as *mean* or *resolved kinetic energy*), residual turbulent (or subgrid) kinetic energy k, and $E_{i+p} = c_p\overline{\theta} - z\overline{b} + gz$, the sum of averaged internal energy and potential energy, where b is the buoyancy acceleration (see Tailleux and Dubos (2024) and Part I). We were able to de-

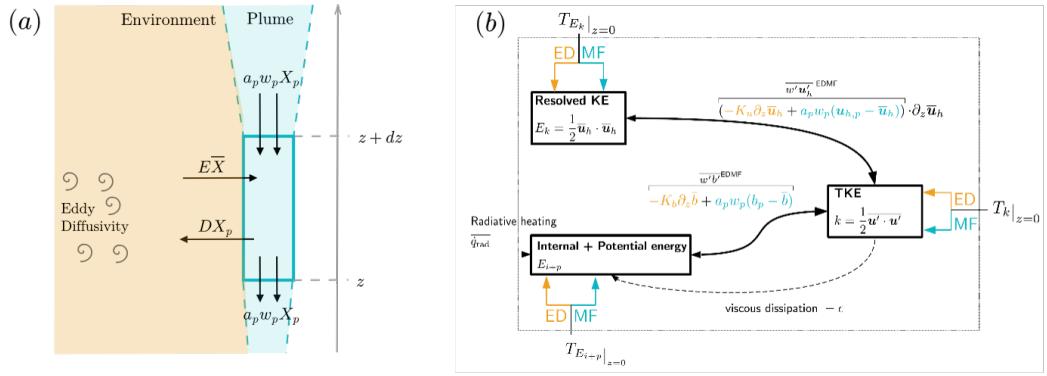

Figure 1: Schematic representation of (a) plume tracer budget, aside with eddy-diffusivity in the environment (b) energy budgets in EDMF.

rive closed energy budgets, including the TKE equation in Part I (see fig. 1(b))

$$\begin{cases} \partial_t E_k + \partial_z T_{E_k} & = -K_u(\partial_z \overline{\boldsymbol{u}}_h)^2 + a_p w_p(\boldsymbol{u}_{h,p} - \overline{\boldsymbol{u}}_h) \cdot \partial_z \overline{\boldsymbol{u}}_h \\ \partial_t k + \partial_z T_k & = -K_\phi \partial_z \overline{b} + a_p w_p(b_p - \overline{b}) + K_u(\partial_z \overline{\boldsymbol{u}}_h)^2 - a_p w_p(\boldsymbol{u}_{h,p} - \overline{\boldsymbol{u}}_h) \cdot \partial_z \overline{\boldsymbol{u}}_h - \overline{\epsilon} \\ \partial_t E_{i+p} + \partial_z T_{E_{i+p}} & = -\left(-K_\phi \partial_z \overline{b} + a_p w_p(b_p - \overline{b})\right) + \overline{\epsilon} \end{cases} \tag{2}$$

where

$$T_{E_k} = (-K_u \partial_z \overline{\boldsymbol{u}}_h + a_p w_p(\boldsymbol{u}_{h,p} - \overline{\boldsymbol{u}}_h)) \cdot \overline{\boldsymbol{u}}_h \tag{3}$$

$$T_{E_{i+p}} = -\partial_z \left(c_p \left(-K_\phi \partial_z \overline{\theta} + a_p w_p(\theta_p - \overline{\theta})\right) - z\left(-K_\phi \partial_z \overline{b} + a_p w_p(b_p - \overline{b})\right)\right) \tag{4}$$

Based on conditional sampling of convective plumes, we propose a new formulation for the transport of TKE, T_k, in section 2.

Finally plume-related equations can be derived using a two-fluid averaging procedure of the original unaveraged equations. Standard EDMF formulations – followed in this study – rely on two main assumptions (see e.g. Part I and Yano (2014)): (i) stationarity of the plume, i.e. $\partial_t(a_p X_p) \ll \partial_z(a_p w_p X_p)$; (ii) small-area occupied by the plume, i.e. considering $a_p \ll 1$ while keeping order one contribution of mass-flux $a_p w_p$ and source terms. Thus the generic plume equation assumes a balance between vertical plume advection, horizontal entrainment (E) of environment fluid into the plume or detrainment (D) of plume fluid into the environment, and potential additional sources (see fig. 1(a)),

$$\partial_z(a_p w_p X_p) = E\overline{X} - DX_p + S_{X,p}$$

The comprehensive plume model equations are given in Table 1. A description of the closures are exposed in Part I.

The paper is organized as follows. In section 2 we derive a new closure for the turbulent transport of TKE. In section 3 we describe the two idealized LES test cases and assess the validity of hypotheses used in the derivation of the MF scheme. In section 4 we derive a discretization that preserves the energetically consistent nature of EDMF equations. In section 5 we evaluate the SCM against LES and realistic data, assess the impact of different parameterization aspects, and quantify energy biases of inconsistent formulations, including double-counting errors due to inconsistent boundary conditions.

$\partial_z(a_p w_p)$	$= E - D$	Plume area conservation equation
$a_p w_p \partial_z \theta_p$	$= E(\overline{\theta} - \theta_p)$	Plume temperature equation
$a_p w_p \partial_z S_p$	$= E(\overline{S} - S_p)$	Plume salinity equation
$a_p w_p \partial_z \boldsymbol{u}_{h,p}$	$= E(\overline{\boldsymbol{u}}_h - \boldsymbol{u}_{h,p}) + a_p w_p C_u \partial_z \overline{\boldsymbol{u}}_h$	Plume horizontal momentum equation
$a_p w_p \partial_z w_p$	$= -bEw_p + a_p \left[aB_p + \frac{b'}{h}(w_p)^2 \right]$	Plume vertical velocity equation
B_p	$= b_{\text{eos}}(\theta_p, S_p) - b_{\text{eos}}(\overline{\theta}, \overline{S})$	Buoyancy forcing term
E	$= a_p C_\epsilon \max(0, \partial_z w_p)$	Lateral entrainment closure
D	$= -a_p C_\delta \min(0, \partial_z w_p) - a_p w_p \delta_0 \frac{1}{h}$	Lateral detrainment closure

Table 1: Summary of the plume equations in the small area limit under the steady plume hypothesis. $C_u, a, b, b', \beta_1, \beta_2, \delta_0$ are dimensionless parameters. h is an estimate of the mixed layer depth, computed as the depth at which $w_p(z = -h) = 0$. "eos" stands for "equation of state".

2 A new closure for the transport of TKE

The redistribution terms of TKE are often little discussed in turbulence parameterization since they do not contribute directly to the vertically integrated energy budgets. However, they are of great importance in convective conditions where non-local transport dominates (Witek et al., 2011). For instance, TKE produced close to the surface due to destabilizing buoyancy fluxes is then transported by coherent plumes into the mixed layer. Taking into account MF transport of TKE is thus essential to achieve local energetic consistency, and model accurately TKE at any level z.

Turbulent fluxes of TKE arise from the contribution of a TKE transport term, a pressure redistribution term and a viscous flux,

$$T_k = \frac{1}{2}\overline{w' \boldsymbol{u}' \cdot \boldsymbol{u}'} + \frac{1}{\rho_0}\overline{w' p'} - \nu \partial_z k \tag{5}$$

For oceanic flows, the viscous flux is negligibly small and will be omitted. We will assume that the pressure redistribution term can be incorporated into the transport term of TKE assuming proportionality, as it is usually done in CBL schemes (e.g. Mellor, 1973). In numerical models, TKE transport is usually parameterized via K-diffusion, namely

$$\partial_z \left(\overline{w' \frac{\boldsymbol{u}' \cdot \boldsymbol{u}'}{2}} \right) \simeq -\partial_z (K_k \partial_z k) \tag{6}$$

Alternatively, to derive a mass-flux based closure we can apply the plume/environment decomposition of the horizontal average to get the exact relation

$$\begin{aligned} \overline{w' \frac{\boldsymbol{u}' \cdot \boldsymbol{u}'}{2}} \quad = \quad & \sum_{i=e,p} \underbrace{a_i \frac{1}{2} \overline{\boldsymbol{u}_i' \cdot \boldsymbol{u}_i' w_i'}}_{\mathrm{I}_i} + \underbrace{a_i (\boldsymbol{u}_i - \overline{\boldsymbol{u}}) \cdot \overline{\boldsymbol{u}_i' w_i'}}_{\mathrm{II}_i} \\ & + \underbrace{a_i (w_i - \overline{w}) \frac{1}{2} \overline{\boldsymbol{u}_i' \cdot \boldsymbol{u}_i'}}_{\mathrm{III}_i} + \underbrace{a_i \frac{1}{2} \|\boldsymbol{u}_i - \overline{\boldsymbol{u}}\|^2 (w_i - \overline{w})}_{\mathrm{IV}_i} \end{aligned} \tag{7}$$

where the subscript e denotes variables of the environment, and the sudomain moments are defined as

$$\overline{w_i' u_i'} = \int_{A_i} (w - w_i)(u - u_j)\,\mathrm{d}x\mathrm{d}y \tag{8}$$

where A_i $(i = e, p)$ is the area occupied by the environment or the plume. Terms of (7) are interpreted as follow: I_i is an intra-subdomain turbulent TKE transport; II_i is a transport of Reynolds stress by the coherent velocities; III_i is a transport of subdomain TKE by the coherent velocities (*i.e.* transport of TKE by mass-flux); IV_i is a transport of convective kinetic energy by coherent velocities. Based on LES simulations (see Sec. 3.3), we found that: (i) I_p can be neglected, consistently with the small area limit; (ii) II_e and II_p are almost compensating, thus the sum $\mathrm{II}_e + \mathrm{II}_p$ can be neglected. We can conveniently reformulate the remaining terms as (see Appendix B for details):

$$\mathrm{III}_e + \mathrm{III}_p + \mathrm{IV}_e + \mathrm{IV}_p = a_p w_p \frac{1}{1 - a_p} \left(k_p + \frac{1}{2} \|\boldsymbol{u}_p - \overline{\boldsymbol{u}}\|^2 - k \right) \tag{9}$$

where sub-domain TKE are $k_i := 1/2\overline{\boldsymbol{u}_i' \cdot \boldsymbol{u}_i'}$ $(i = e, p)$ and TKE can be decomposed as the sum of domain-averaged TKEs and sub-domain TKEs:

$$k = \frac{1}{2} a_e \|\boldsymbol{u}_e - \overline{\boldsymbol{u}}\|^2 + a_e k_e + \frac{1}{2} a_p \|\boldsymbol{u}_p - \overline{\boldsymbol{u}}\|^2 + a_p k_p \tag{10}$$

In EDMF closures, turbulence is assumed isotropic in the environment, thus we close $\frac{1}{2}\overline{\boldsymbol{u}_e' \cdot \boldsymbol{u}_e' w_e'}$ with K-diffusion, similar to the standard practice for TKE-only schemes. Then assuming $\frac{1}{1-a_p} \simeq 1$ (i.e. the small area limit) we have

$$\overline{w' \frac{\boldsymbol{u}' \cdot \boldsymbol{u}'}{2}} = \underbrace{-K_k \partial_z k}_{\text{ED}} + \underbrace{\overbrace{a_p w_p (k_p - k)}^{\text{Han \& Bretherton 2019}} + \overbrace{a_p w_p^3}^{\text{Witek et al. 2011}} + \frac{a_p w_p}{2} \|\boldsymbol{u}_{h,p} - \overline{\boldsymbol{u}}_h\|^2}_{\text{new EDMF}} \tag{11}$$

It is interesting to note that we can recover existing formulations from the proposed closure (11): if $a_p w_p = 0$ it boils down to the classical eddy-diffusivity closure; if $k_p = k$ and $\boldsymbol{u}_{h,p} = \overline{\boldsymbol{u}}_h$ the term $1/2 w_p^3$ proposed by Witek et al. (2011) is recovered; if TKE is treated as a tracer transported by the plume then the formulation proposed by Han and Bretherton (2019) is recovered. However, we should mention that these latter treatment seems incorrect because $\overline{w' \boldsymbol{u}' \cdot \boldsymbol{u}'/2}$ is not a second-order moment, but a third-order moment which requires a proper treatment as seen in (7).

Finally, one still needs to provide a value for k_p. Without any assumption, its prognostic equation reads (Tan et al., 2018, eq. (11))

$$\begin{aligned}
\partial_t (a_p k_p) + \partial_z (a_p w_p k_p) \quad = \quad & -a_p \overline{w_p' \boldsymbol{u}_{h,p}'} \cdot \partial_z \boldsymbol{u}_{h,p} + a_p \overline{w_p' b_p'} \\
& + E \left(k_e + \frac{1}{2} \|\boldsymbol{u}_e - \boldsymbol{u}_p\|^2 \right) - D k_p \\
& - \partial_z \left(a_p \overline{w_p' \frac{\boldsymbol{u}_p' \cdot \boldsymbol{u}_p'}{2}} + a_p \overline{\boldsymbol{u}_p' \cdot \frac{1}{\rho_0} (\nabla p^\dagger)_p'} \right) \\
& - a_p \epsilon_p
\end{aligned}$$

Consistent with the neglect of subplume fluxes and temporal tendency in EDMF (see Part I or Tan et al. (2018)), we propose as a first attempt to retain advection, entrainment, detrainment and dissipation terms, which lead to the simplified form of the pre-

vious equation:

$$\begin{aligned}
\partial_z(a_p w_p k_p) &= E\left(k_e + \frac{1}{2}\|\boldsymbol{u}_e - \boldsymbol{u}_p\|^2\right) - Dk_p - a_p\epsilon_p \\
&= E\left(\overbrace{\frac{1}{1-a_p}k - \frac{a_p}{1-a_p}(k_p + \frac{1}{2}\|\boldsymbol{u}_p - \overline{\boldsymbol{u}}\|^2)}^{k_e} + \overbrace{\frac{1}{(1-a_p)^2}\frac{1}{2}\|\boldsymbol{u}_p - \overline{\boldsymbol{u}}\|^2}^{\frac{1}{2}\|\boldsymbol{u}_e - \boldsymbol{u}_p\|^2}\right) \\
&\qquad -Dk_p - a_p\epsilon_p \\
&= E\frac{1}{1-a_p}\left(k - a_p k_p + \left[1 + \frac{a_p^2}{1-a_p}\right]\frac{1}{2}\|\boldsymbol{u}_p - \overline{\boldsymbol{u}}\|^2\right) - Dk_p - a_p\epsilon_p
\end{aligned}$$

where we have used the identity $\|\boldsymbol{u}_e - \boldsymbol{u}_p\|^2 = \frac{1}{(1-a_p)^2}\|\boldsymbol{u}_p - \overline{\boldsymbol{u}}\|^2$ and substituted k_e using (10). Using area conservation, we get the advective form

$$a_p w_p \partial_z k_p = E\frac{1}{1-a_p}\left(k - k_p + \left[1 + \frac{a_p^2}{1-a_p}\right]\frac{1}{2}\|\boldsymbol{u}_p - \overline{\boldsymbol{u}}\|^2\right) - a_p\epsilon_p \tag{12}$$

Finally assuming $\frac{1}{1-a_p} \simeq 1$ and $a_p^2 \ll a_p$ (i.e. the small area limit) we have

$$a_p w_p \partial_z k_p = E\left(k - k_p + \frac{1}{2}\|\boldsymbol{u}_p - \overline{\boldsymbol{u}}\|^2\right) - a_p\epsilon_p \tag{13}$$

where the closure for dissipation is taken as $\epsilon_p = c_\epsilon / l_\epsilon (k_p)^{2/3}$ (c_ϵ is a constant and l_ϵ is a length scale, see Appendix A). As a summary, the proposed closure of TKE transport is given by

$$\begin{cases} \overline{w'\frac{\boldsymbol{u}'\cdot\boldsymbol{u}'}{2}} = & -K_k\partial_z k + a_p w_p\left(k_p - k + \frac{1}{2}\|\boldsymbol{u}_p - \overline{\boldsymbol{u}}\|^2\right) \\ a_p w_p \partial_z k_p = & E\left(k - k_p + \frac{1}{2}\|\boldsymbol{u}_p - \overline{\boldsymbol{u}}\|^2\right) - a_p\epsilon_p \end{cases} \tag{14}$$

We will now use LES to evaluate EDMF assumptions and the new closure of TKE transport.

3 Test cases description and validation of formulation

In this section we describe the reference idealized cases that will be further used in the study; then we describe the LES model and the conditional sampling technique used to identify convective plumes; finally we evaluate EDMF assumptions and the new closure of TKE transport.

3.1 Description of idealized cases

The two idealized cases considered are reminiscent of typical convective conditions in the ocean (e.g. Marshall & Schott, 1999), where convection into a initially resting ocean of constant stratification $\Delta\theta = 1\,\mathrm{K}/1000\,\mathrm{m}$ (corresponding $N_0^2 = 1.962 \times 10^{-6}\,\mathrm{s}^{-2}$) is triggered by a surface cooling of $Q_0 = -500\,\mathrm{W\,m^{-2}}$ (corresponding to a surface buoyancy loss of $B_0 = -2.456\times10^{-7}\,\mathrm{m^2 s^{-3}}$). In both cases, salinity is kept uniform at $S = 32.6\,\mathrm{psu}$. The first case (FC500) consists of free convection, where no wind stress is applied. In the second idealized case (W005_C500) a uniform wind stress along the meridional direction, of magnitude $(u_*^a)^2 = 0.05\,\mathrm{m^2\,s^{-2}}$, is applied. A summary of the parameters for each case can be found in table 2. To characterize wind-shear effects, we introduce the Froude number (Haghshenas & Mellado, 2019a)

$$Fr_* = \frac{u_*^o}{N_0 L_0} \tag{15}$$

Table 2: Idealized cases parameters

Case	Q_0 ($\mathrm{W\,m^{-2}}$)	$(u_*^a)^2$ ($\mathrm{m^2\,s^{-2}}$)	N_0^2 ($\mathrm{s^{-2}}$)	t_f (h)	Fr_*
FC500	-500	0	1.962×10^{-6}	72	0
W005_C500	-500	0.05	1.962×10^{-6}	72	0.56

where the length scale $L_0 = (B_0/N_0^3)^{1/2}$ can be interpreted as an Ozmidov scale $(\epsilon/N^3)^{1/2}$ (Garcia & Mellado, 2014) which is a measure of the smallest eddy size affected by a background stratification N^2 in a turbulent field characterized by a viscous dissipation rate ϵ. After $t_f = 72\,\mathrm{h}$ of simulation leading to a mixed layer depth h (defined as the depth at which the buoyancy flux is minimum) of several hundred meters, various non-dimensional numbers can be used to characterize the flow. Their values can be found in Tab. 3. The ratio of the mixed layer depth to the Obukhov length (Obukhov (1971) and Zheng et al. (2021) in the oceanic context) h/L_{Ob}, where

$$L_{Ob} = \frac{(u_*^o)^3}{-B_0}$$

is an estimate of the depth at which the production of TKE by turbulent shear is of the same order of magnitude as the production of TKE by buoyancy fluxes. Noting $w_* = (-B_0 h)^{1/3}$ the convective velocity scale (Deardorff, 1970), we get

$$\frac{h}{L_{Ob}} = \left(\frac{w_*}{u_*}\right)^3 \tag{16}$$

We also recall that the oceanic friction velocity u_*^o satisfies $\rho_o (u_*^o)^2 = \rho_a (u_*^a)^2$. The Richardson number at the mixed layer base,

$$Ri_h = \frac{N_0^2}{\left(\frac{u_*^o}{h}\right)^2}$$

measures the destabilization by surface shear stresses of a stably stratified water column. At $t_f = 72\,\mathrm{h}$, the case W005_C500 can be described by $h/L_{Ob} \simeq 5.7$ and $Ri_h \simeq 310$, which corresponds to a regime of strong deepening of the MLD according to Legay et al. (2023). Finally, for free convection cases (no wind) a convective Richardson number can be built as

$$Ri_* = \frac{N_0^2}{(w_*/h)^2} = \frac{N_0^2 h^{4/3}}{(-B_0)^{2/3}} = Ri_h \left(\frac{L_{Ob}}{h}\right)^{2/3}$$

It can be interpreted as follows. The time evolution of the mixed layer depth can be accurately described by the scaling (Turner, 1979; Van Roekel et al., 2018)

$$h \propto h_{\mathrm{enc}} \tag{17}$$

where the *encroachment* depth is $h_{\mathrm{enc}}(t) := \sqrt{2\frac{(-B_0)}{N_0^2}t}$. Then the ratio of the entrainment velocity $w_e = \frac{d}{dt}h$ to the convective velocity $w_* = (-B_0 h)^{1/3}$ reads

$$\frac{w_e}{w_*} \propto Ri_*^{-1} \tag{18}$$

Table 3: Idealized cases non-dimensional parameters after 72 h of simulation

Case	h/L_{Ob}	Ri_h	Ri_*
FC500	∞	∞	97
W05_C500	5.7	310	97

3.2 LES model description and conditional sampling

The LES data have been generated by the non-hydrostatic model Méso-NH (Lac et al., 2018), using the Ocean-LES version developed by Jean-Luc Redelsperger. It is solving an anelastic Lipps-Hemler system adapted to the ocean, along with a linearized equation of state. The model uses a second-order Runge-Kutta time stepping and spatial discretization of advection operators is performed with a fourth-order centered scheme. Explicit subgrid scale closures are computed via a 3-D turbulence scheme based on a prognostic equation of the subgrid turbulent kinetic energy using a mixing-length scale, computed from the volume of a grid cell (Cuxart et al., 2000). The domain size is 1000 m on the vertical and 7.5 km×7.5 km on the horizontal, where doubly periodic conditions are applied. A resolution of 10 m on the vertical and 15 m on the horizontal is used. Each configuration is run for 72 h with a time-step of 10 s. To assess the quality of the simulations, we checked that the subgrid TKE was never exceeding 20% of the TKE explicitly resolved by the LES (Pope, 2004). Via analysis of the total TKE budget, we checked that a quasi-steady regime is reached after a few hours of simulation (e.g. Garcia & Mellado, 2014). Moreover, at the end of the simulations, the typical size of coherent structures, which can be quantified by the horizontal integral length scale in the bulk of the mixed layer, is of the order $O(500\,\mathrm{m}) \ll 7.5\,\mathrm{km}$. This suggests that the horizontal domain is large enough to provide a satisfactory statistical sampling of turbulent structures.

To identify plumes, we use a velocity-based conditional sampling adapted from Pergaud et al. (2009), where the plume area is defined as

$$A_p(z,t) = \left\{ (x,y,z,t) \text{ such that } \overline{w}(z,t) - w(x,y,z,t) > m \times \max(\sqrt{\overline{w^{2\prime}}}(z,t), \sigma_{\min}(z,t)) \right\} \quad (19)$$

where the minimum standard deviation is chosen as $\sigma_{\min}(z,t) = 0.05/(-z)\int_z^0 \sqrt{\overline{w^{2\prime}}}(z',t)\,\mathrm{d}z'$. We checked that the further conclusions were not sensitive to m, and fixed $m = 1$. We do not use the tracer-based sampling of Couvreux et al. (2010) since it is valid only for small variations of the mixed layer depth. We neither utilize the "strong updraft" sampling of (Siebesma et al., 2007) since it assumes that a_p is a given constant. However, we checked that similar conclusions could be drawn from such samplings (not shown).

3.3 Evaluation of the steady plume and small area hypotheses

In this section, we directly evaluate the validity of the main assumptions of EDMF scheme, namely that plumes are stationary and that their area is negligible compared to the total grid area.Figs. 2 and 3 show that the plume temporal tendency terms are $O(10^{-1}--10^{-2})$ smaller than plume advective terms which is consistent with the scaling in $1/(N_0 t)$ derived in Part I. This justifies the use of the steady plume hypothesis. Figs. 4 and 5 show vertical profiles of temperature, vertical velocity, plume fractional area, and temperature flux for the idealized cases FC500 and W005_C500. Values of $a_p(z)$ range between 10% and 20% of the total area, as exposed in previous studies (e.g. Couvreux et al., 2010). Thus the assumption of modeling a small plume area is not really accurate. This justifies questioning the relevance of this assumption and considering the system described in 5.3, in which a_p is not considered small anymore. The convective

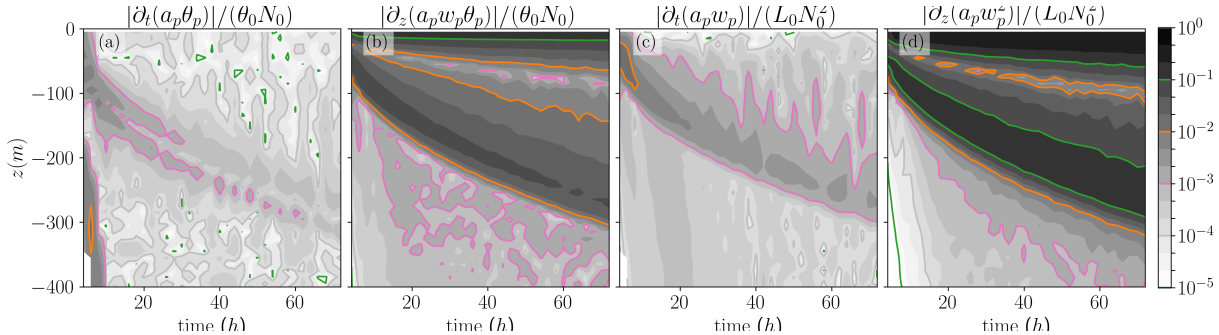

Figure 2: Temporal evolution of the normalized plume tendency $\partial_t(a_p X_p)$ and plume advection $\partial_z(a_p w_p X_p)$ terms ($X = \theta, w$), for the case FC500. Colored lines indicate thresholds to each power of ten.

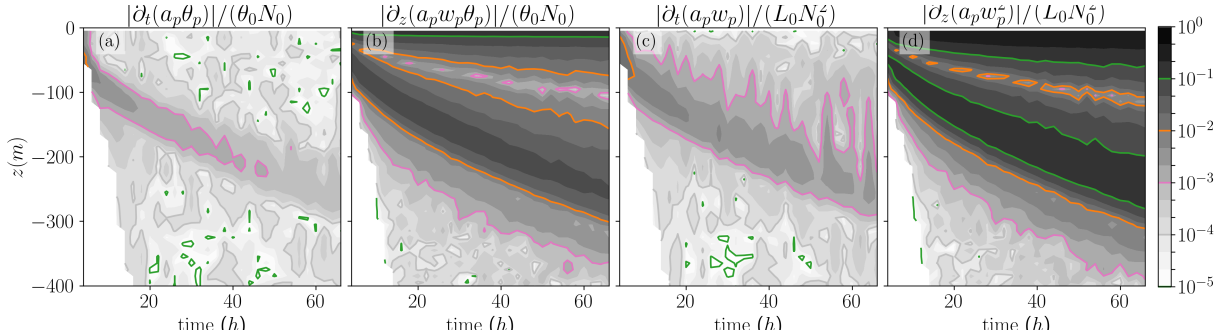

Figure 3: Same as figure 2 for the case W005_C500.

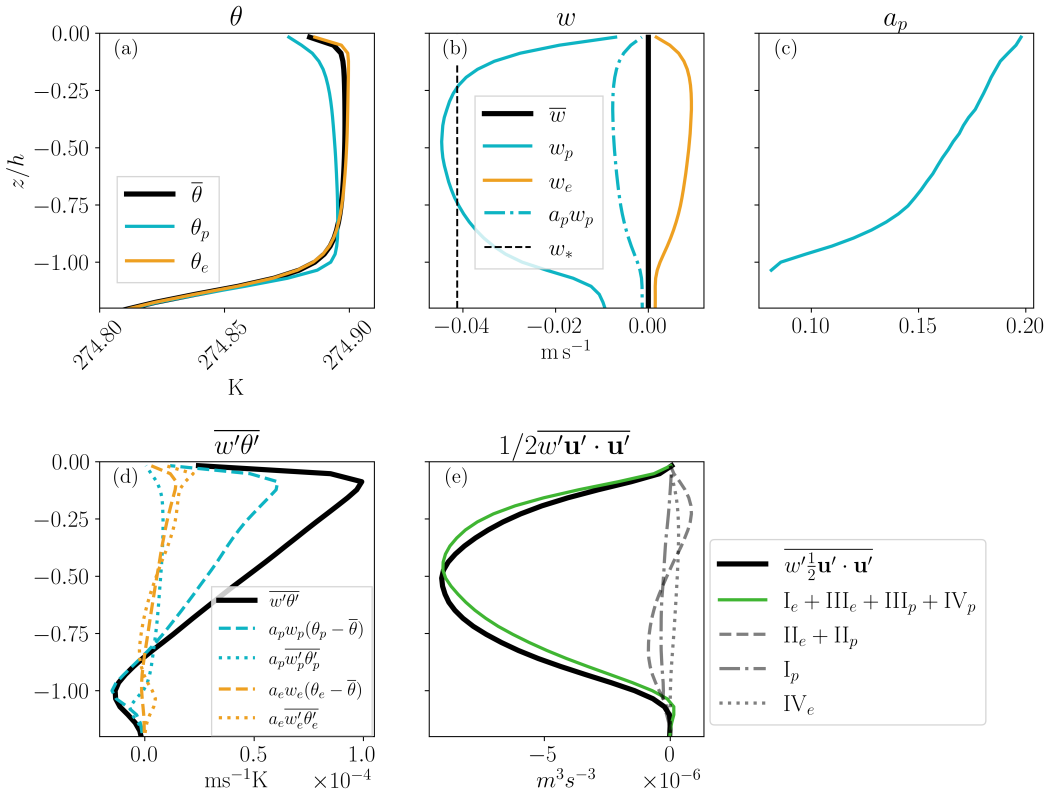

Figure 4: LES vertical profiles of (a) temperature, (b) vertical velocities, (c) plume fractional area, (d) temperature flux and (e) TKE flux for the FC500 case after 72 h of simulation. For each field, the black line represents a horizontal average over the whole grid cell, the blue line represents an average over the plume area and the orange line represents an average over the environment area. In panel (b) the blue dotted line represents $a_p w_p$, and the gray dashed line represents the value of the free convective velocity scale w_*. In panel (d), total flux is in black, plume fluxes in blue (MF is dashed and subplume is dotted), and environment fluxes in orange (same linestyles). In panel (e) are represented the total flux (black) and the contributions from the combined terms $\mathrm{I}_e + \mathrm{III}_e + \mathrm{III}_p + \mathrm{IV}_p$ (blue), $\mathrm{II}_e + \mathrm{II}_p$ (dashed gray), I_p (dash-dotted gray) and III_p (dotted gray) (see 2 for details).

velocity w_* is found to be a good estimate of the plume vertical velocity w_p (panel (b)). The contribution of the mass-flux term $a_p w_p(\theta_p - \overline{\theta})$ (panel (d)) to the total temperature flux is increasing with depth, until reaching a quasi-perfect match in the entrainment layer. The rough validity of the assumption $a_p w_p(\theta_p - \overline{\theta}) \gg a_p\overline{w'_p\theta'_p}, a_e w_e(\theta_e - \overline{\theta})$ is consistent with the rough validity of $a_p \ll 1$. The plume/environment decomposition of the vertical transport of TKE $1/2\overline{w'\boldsymbol{u}'\cdot\boldsymbol{u}'}$ is presented in Figs. 4(e) and 5(e). The dominant terms exposed in eq. (9) explain well the total flux.

Thanks to LES, we have assessed the validity of hypotheses used to derive the continuous formulation of our energetically consistent EDMF scheme. We now turn to the discretization of such scheme.

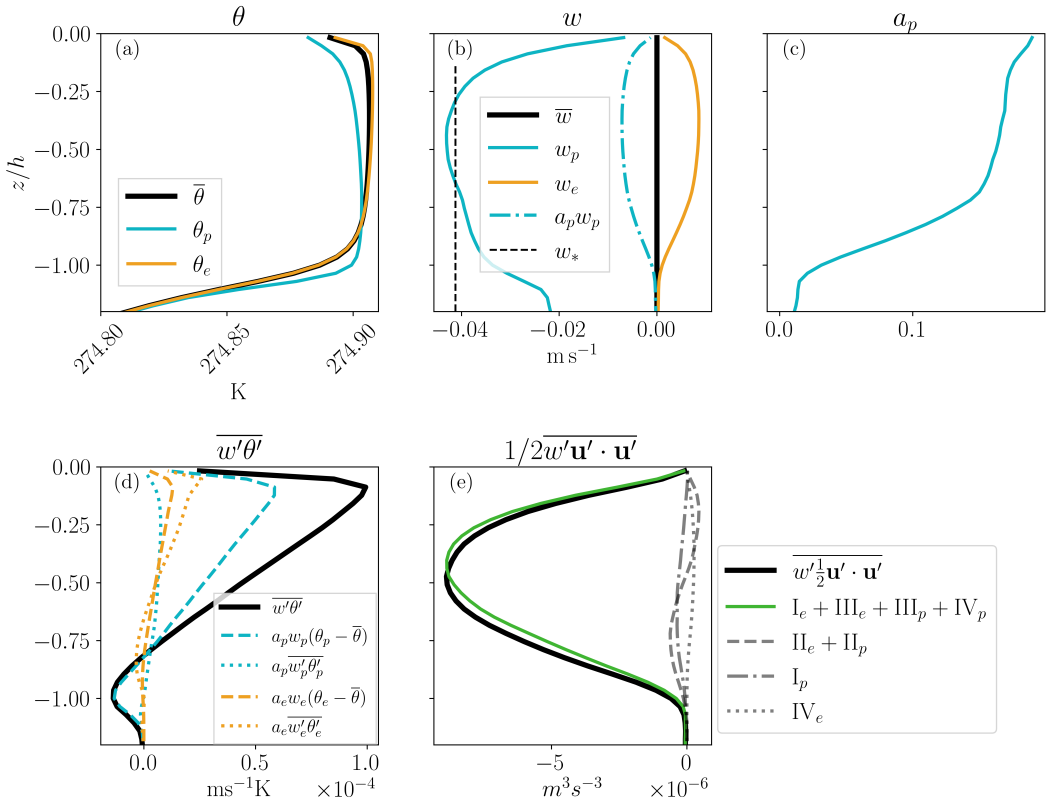

Figure 5: Same as figure 4 for the case W005_C500.

4 Discretization of energetically consistent EDMF equations

In this section, we derive a discretization that satisfies the conservative energy exchange described in Part I (see also the introduction in section 1) at a discrete level when using EDMF. This is achieved through discrete mean kinetic, turbulent kinetic, and potential energy budgets. This type of approach has already been proposed by Burchard (2002) in the ED case to derive an energy-conserving discretization method for the shear and buoyancy production terms in the TKE. In what follows, we generalize this approach to the EDMF case. This section is divided into 2 subsections, the first about the coupling between ED and MF schemes within the time-stepping algorithm and the second about an energy-conserving discretization of TKE production and destruction terms. For readers interested in a practical implementation of the proposed EDMF scheme in a numerical model, full details of a simple discretization of the MF equations are given in Appendix C including the way the mixed layer depth h is computed. The proposed discretization guarantees that w_p is strictly negative, that a_p is bounded between 0 and 1, and that the continuity and tracer equations are compatible, without the need for an iterative solution procedure.

4.1 Coupling ED and MF schemes

In the EDMF approach, the usual vertical diffusion/viscous subgrid terms are completed by an advective term so that the following equation must be advanced in time (with $X = u, v, \theta, S$):

$$\partial_t \overline{X} = \partial_z \left(K_X \partial_z \overline{X} \right) - \partial_z \left(a_p w_p (X_p - \overline{X}) \right) \tag{20}$$

This amounts to couple a boundary layer scheme which provides K_X and a convection scheme which provides $a_p w_p$ and X_p. The numerical treatment of such coupling can be approached in 2 ways: either by integrating the 2 schemes sequentially or in parallel. For the numerical experiments discussed in Sec. 5 we chose a *boundary layer-then-convection* strategy corresponding to the following temporal integration for the single-column model (leaving aside the Coriolis and solar penetration terms, and for $\phi = \theta, S$)

$$\begin{aligned}
&\text{ED step}\\
\phi^{n+1,\star} &= \phi^n + \Delta t \partial_z \left(K_\phi(k^n, b^n) \partial_z \phi^{n+1,\star} \right)\\
\boldsymbol{u}_h^{n+1,\star} &= \boldsymbol{u}_h^n + \Delta t \partial_z \left(K_{\boldsymbol{u}}(k^n, b^n) \partial_z \boldsymbol{u}_h^{n+1,\star} \right)\\
b^{n+1,\star} &= b_{\text{eos}}(\phi^{n+1,\star})\\
&\text{MF step}\\
[a_p, w_p, \phi_p, \boldsymbol{u}_{h,p}, k_p, B_p] &= \text{MF}(\phi^{n+1,\star}, b^{n+1,\star}, \boldsymbol{u}_h^{n+1,\star})\\
\phi^{n+1} &= \phi^{n+1,\star} - \Delta t \partial_z \left(a_p w_p (\phi_p - \phi^{n+1,\star}) \right)\\
\boldsymbol{u}_h^{n+1} &= \boldsymbol{u}_h^{n+1,\star} - \Delta t \partial_z \left(a_p w_p (\boldsymbol{u}_{h,p} - \boldsymbol{u}_h^{n+1,\star}) \right)\\
&\text{TKE update}\\
k^{n+1} &= k^n + \Delta t \partial_z \left(K_k(k^n, b^n) \partial_z k^{n+1} \right) + \mathcal{F}_k(b^{n+1}, \boldsymbol{u}_h^{n+1}, \boldsymbol{u}_h^n, a_p, w_p, \boldsymbol{u}_{h,p}, k_p, B_p)
\end{aligned}$$

where the MF(.) function represents the computation of mass-flux quantities as described in Appendix C and $\mathcal{F}_k$ contains the TKE transport and forcing terms whose discrete expression will be given in next subsection. In oceanic models, the "ED step" is classically computed using an Euler backward scheme. With the proposed approach, the convection scheme takes as input a state already updated by the boundary layer scheme (and by the solar penetration and non-solar surface heat flux which are applied during the "ED step") The convection scheme therefore uses a state whose static stability is representative of the current time-step and external forcing. Ultimately, with the proposed ap-

proach, the various stages can be expressed directly as follows

$$\begin{aligned}\phi^{n+1} &= \phi^n + \Delta t \partial_z \left(K_\phi \partial_z \phi^{n+1,\star} - a_p w_p (\phi_p - \phi^{n+1,\star}) \right) \\ [a_p, w_p, \phi_p] &= \mathrm{MF}(\phi^{n+1,\star})\end{aligned}$$

which reflects the fact that the ED part and the MF part are properly synchronized in time, as they consider the same mean fields. In the case where stratification is stable throughout the column, the mass flux scheme returns a zero fraction a_p and we simply obtain $\phi^{n+1} = \phi^{n+1,\star}$.

On the other hand, the approach of simultaneously considering the ED and MF parts in a single tridiagonal problem (a.k.a. the *boundary layer-and-convection* strategy, e.g. Giordani et al. (2020)) would lead to

$$\begin{aligned}\phi^{n+1} &= \phi^n + \Delta t \left(K_\phi \partial_z \phi^{n+1} - a_p w_p (\phi_p - \phi^{n+1}) \right) \\ [a_p, w_p, \phi_p] &= \mathrm{MF}(\phi^n)\end{aligned}$$

In this case, the mass flux variables are computed using mean fields at time n. Indeed ϕ_p has been computed using ϕ^n while it is applied at time $n+1$. However, this strategy has the advantage of being unconditionally stable while the *boundary layer-then-convection* strategy is conditionally stable[1]. Based on the sequential integration of ED and MF components, we now turn to the spatial discretization of an energetically coherent EDMF scheme.

4.2 Energy consistent discretization of TKE dissipation and production terms

We consider the standard grid arrangement used in oceanic models which are usually discretized on a Lorenz grid in the vertical (density is located in the center of the cells on the vertical). We consider N grid cells in the vertical with thickness $\Delta z_j = z_{j+1/2} - z_{j-1/2}$ ($z_{1/2} = -H$ and $z_{N+1/2} = 0$ the surface) such that $\sum_{j=1}^{N} \Delta z_j = -H$. Traditionally, turbulent quantities like turbulent kinetic energy k and eddy diffusivities K_X are naturally located on the interfaces at $z_{j+1/2}$ to avoid interpolations when computing the vertical gradients of the turbulent fluxes. For the discrete values, not to interfere with the grid indices, the subscript p for the plume quantities is now a superscript such that plume quantities are now noted $X^p_{j+1/2} = X_p(z = z_{j+1/2})$. In the following, we consider that the plume quantities and k are discretized at cell interfaces and the mean quantities are discretized at cell centers.

The turbulent flux $\overline{w'X'}$ (for $X = u, b, \theta$) are discretized at cell interfaces as

$$\left(\overline{w'X'}\right)_{j+1/2} = \mathcal{J}^X_{j+1/2} = -K^X_{j+1/2} \frac{(\delta_z X)^{n+1,\star}_{j+1/2}}{\Delta z_{j+1/2}} + (a^p w^p)_{j+1/2} \left(X^p_{j+1/2} - X^{n+1,\star}_j \right)$$

with $(\delta_z X)^{n+1,\star}_{j+1/2} = X^{n+1,\star}_{j+1} - X^{n+1,\star}_j$ and $[a^p, w^p, X^p] = \mathrm{MF}(X^{n+1,\star})$.

4.2.1 Discrete mean kinetic energy equation

Multiplying the discrete equation for u_j by $u^{n+1/2}_j = \left(u^{n+1}_j + u^n_j\right)/2$ we obtain

$$\frac{(u^{n+1}_j)^2 - (u^n_j)^2}{2\Delta t} = -\frac{u^{n+1/2}_j}{\Delta z_j} \left[\mathcal{J}^u_{j+1/2} - \mathcal{J}^u_{j-1/2} \right]$$

[1] The stability constraint is given by $-a_p w_p \leq \frac{\Delta z}{2\Delta t}\left(1 + \sqrt{1 + 8\frac{K\Delta t}{\Delta z^2}}\right)$ which is obtained through standard Von Neumann stability analysis.

After some simple algebra[2] the mean kinetic energy equation can be expressed as

$$\frac{(u_j^{n+1})^2-(u_j^n)^2}{2\Delta t}+\frac{1}{\Delta z_j}\left(u_{j+1/2}^{n+1/2}\mathcal{J}_{j+1/2}^u-u_{j-1/2}^{n+1/2}\mathcal{J}_{j-1/2}^u\right)=\frac{1}{2\Delta z_j}\left\{(\delta_z u)_{j+1/2}^{n+1/2}\mathcal{J}_{j+1/2}^u+(\delta_z u)_{j-1/2}^{n+1/2}\mathcal{J}_{j-1/2}^u\right\} \tag{21}$$

where the terms in curly brackets on the right-hand side contribute to the discrete expressions of the ED and MF TKE production terms by shear while the flux divergence term corresponds to the $\partial_z T_{E_k}$ term in (2). The vertically integrated discrete budget reads

$$\sum_{j=1}^{N}\Delta z_j\left(\frac{(u_j^{n+1})^2-(u_j^n)^2}{2\Delta t}\right)+u_{N+1/2}^{n+1/2}\mathcal{J}_{N+1/2}^u-u_{1/2}^{n+1/2}\mathcal{J}_{1/2}^u$$
$$=\frac{1}{2}\left((\delta_z u)_{N+1/2}^{n+1/2}\mathcal{J}_{N+1/2}^u+(\delta_z u)_{1/2}^{n+1/2}\mathcal{J}_{1/2}^u\right)+\sum_{j=1}^{N-1}(\delta_z u)_{j+1/2}^{n+1/2}\mathcal{J}_{j+1/2}^u$$

Boundary condition for the momentum flux are such that the *numerical flux* equals the *physical flux*, i.e. $\mathcal{J}_{N+1/2}^u=-\tau_x/\rho_0$ and $\mathcal{J}_{1/2}^u=0$, where τ_x is the surface momentum stress. For conciseness we assumed a no stress condition at the bottom, and vanishing gradients of momentum at the surface and the boundary as in (Burchard, 2002) (but they could have been kept without additional complications). The vertically integrated discrete budget is thus simplified into

$$\sum_{j=1}^{N}\Delta z_j\left(\frac{(u_j^{n+1})^2-(u_j^n)^2}{2\Delta t}\right)-u_{N+1/2}^{n+1/2}\frac{\tau_x}{\rho_0}=\sum_{j=1}^{N-1}(\delta_z u)_{j+1/2}^{n+1/2}\mathcal{J}_{j+1/2}^u \tag{22}$$

The term on the right-hand side corresponds to a transfer between the mean and turbulent kinetic energies.

4.2.2 Discrete mean internal and potential energy equation

We consider the energy $c_p\overline{\theta}-z\overline{b}$ which satisfies the discrete evolution equation

$$\frac{(c_p\theta-zb)_j^{n+1}-(c_p\theta-zb)_j^n}{\Delta t}=-\frac{c_p}{\Delta z_j}\left[\mathcal{J}_{j+1/2}^\theta-\mathcal{J}_{j-1/2}^\theta\right]+\frac{z_j}{\Delta z_j}\left[\mathcal{J}_{j+1/2}^b-\mathcal{J}_{j-1/2}^b\right]+\epsilon_j$$

After some simple algebra[3], the discrete energy equation can be expressed as

$$\frac{(c_p\theta-zb)_j^{n+1}-(c_p\theta-zb)_j^n}{\Delta t}+\frac{1}{\Delta z_j}\left[\left(c_p\mathcal{J}_{j+1/2}^\theta-z_{j+1/2}\mathcal{J}_{j+1/2}^b\right)-\left(c_p\mathcal{J}_{j-1/2}^\theta-z_{j-1/2}\mathcal{J}_{j-1/2}^b\right)\right]$$
$$=-\frac{1}{2\Delta z_j}\left\{\Delta z_{j+1/2}\mathcal{J}_{j+1/2}^b+\Delta z_{j-1/2}\mathcal{J}_{j-1/2}^b\right\}+\epsilon_j \tag{23}$$

where the terms in curly brackets on the right-hand side contribute to the discrete expressions of the ED and MF TKE buoyancy production/destruction terms while the flux divergence term corresponds to the $\partial_z T_{E_{i+p}}$ term in (2).

Assuming boundary conditions such that no buoyancy/heat flux through the bottom we get

[2] We multiply $\mathcal{J}_{j+1/2}^u$ by $u_j^{n+1/2}=-\frac{1}{2}(\delta_z u)_{j+1/2}^{n+1/2}+u_{j+1/2}^{n+1/2}$ and $\mathcal{J}_{j-1/2}^u$ by $u_j^{n+1/2}=\frac{1}{2}(\delta_z u)_{j-1/2}^{n+1/2}+u_{j-1/2}^{n+1/2}$

[3] We multiply $\mathcal{H}_{j+1/2}^b$ by $z_j=-\frac{1}{2}\Delta z_{j+1/2}+z_{j+1/2}$ and $\mathcal{H}_{j-1/2}^b$ by $z_j=\frac{1}{2}\Delta z_{j-1/2}+z_{j-1/2}$

$$\sum_{j=1}^{N} \Delta z_j \left(\frac{(c_p\theta - zb)_j^{n+1} - (c_p\theta - zb)_j^n}{\Delta t} \right) + c_p \mathcal{J}^{\theta}_{N+1/2} + \frac{1}{2}\Delta z_{N+1/2} \mathcal{J}^{b}_{N+1/2} = -\sum_{j=1}^{N-1} \Delta z_{j+1/2} \mathcal{J}^{b}_{j+1/2} + \sum_{j=1}^{N} \Delta z_j \epsilon_j \quad (24)$$

where we prescribe that the numerical flux equals the "physical" surface flux, i.e. $c_p \mathcal{J}^{\theta}_{N+1/2} + \frac{1}{2}\Delta z_{N+1/2}\mathcal{J}^{b}_{N+1/2} = c_p \overline{w'\theta'}_0 + g\frac{\Delta z_{N+1/2}}{2}\left(\alpha \overline{w'\theta'}_0 - \beta \overline{w'S'}_0\right)$. Note however that inconsistent boundary condition can lead to additional unphysical energy fluxes (see 5.1.2).

4.2.3 Constraints for discrete energetic consistency

In the same spirit as Burchard (2002), the discrete energy budgets (21) and (23) can be used to derive an energy-conserving discretization of the shear and buoyancy production terms for turbulent kinetic energy. As stated above the TKE variable is naturally located at cell interfaces. A discrete expression for its evolution equation is given by :

$$\frac{k^{n+1}_{j+1/2} - k^n_{j+1/2}}{\Delta t} = -\frac{1}{\Delta z_{j+1/2}} \left[\mathcal{G}_{j+1} - \mathcal{G}_j\right] + \mathrm{Sh}_{j+1/2} + \mathcal{B}_{j+1/2} - \epsilon_{j+1/2}$$

The turbulent transport of TKE consistent with (14) is

$$\mathcal{G}_j = -K^k_j \frac{k^{n+1}_{j+1/2} - k^{n+1}_{j-1/2}}{\Delta z_j} + (a^p w^p)_{j+1/2}(k^p_{j+1/2} - k^n_{j-1/2}) + \frac{(a^p w^p)_{j+1/2}}{2}\left((w^p_{j+1/2})^2 + (u^p_{j+1/2} - u^{n+1,\star}_j)^2\right)$$

Using (22) and (24), the constraints for energetic consistency between the mean and turbulent energies at the discrete level lead to

$$\begin{aligned}
\sum_{j=1}^{N-1} \Delta z_{j+1/2} \mathrm{Sh}_{j+1/2} &= -\sum_{j=1}^{N-1} (\delta_z u)^{n+1/2}_{j+1/2} \mathcal{J}^u_{j+1/2} \\
\sum_{j=1}^{N-1} \Delta z_{j+1/2} \mathcal{B}_{j+1/2} &= \sum_{j=1}^{N-1} \Delta z_{j+1/2} \mathcal{J}^b_{j+1/2} \\
\sum_{j=1}^{N-1} \Delta z_{j+1/2} \epsilon_{j+1/2} &= \sum_{j=1}^{N} \Delta z_j \epsilon_j
\end{aligned}$$

Such constraints are satisfied for the following choice of discretizations

$$\begin{cases}
\mathrm{Sh}_{j+1/2} &= \dfrac{(\delta_z u)^{n+1/2}_{j+1/2}}{\Delta z_{j+1/2}} \left(K_{j+1/2} \dfrac{(\delta_z u)^{n+1,\star}_{j+1/2}}{\Delta z_{j+1/2}} - (a_p w_p)_{j+1/2} \left(u^p_{j+1/2} - u^{n+1,\star}_j \right) \right) \\
\mathcal{B}_{j+1/2} &= -K^b_{j+1/2} \left(N^2\right)^{n+1,\star}_{j+1/2} + (a_p w_p)_{j+1/2} \left(b_{\mathrm{eos}}(\phi^p_{j+1/2}) - b_{\mathrm{eos}}(\phi^{n+1,\star}_j) \right) \\
\epsilon_j &= \dfrac{\Delta z_{j+1/2}\epsilon_{j+1/2} + \Delta z_{j-1/2}\epsilon_{j-1/2}}{\Delta z_j}
\end{cases} \quad (25)$$

further assuming that $\epsilon_{1/2} = \epsilon_{N+1/2} = 0$. Considering the discretizations (25), the total energy budget of the water column reads

$$\sum_{j=1}^{N} \Delta z_j \frac{(c_p\theta - zb + u^2/2)^{n+1}_j - (c_p\theta - zb + u^2/2)^n_j}{\Delta t} + \sum_{j=1}^{N-1} \Delta z_{j+1/2} \frac{k^{n+1}_{j+1/2} - k^n_{j+1/2}}{\Delta t} = u^{n+1/2}_{N+1/2} \frac{\tau_x}{\rho_0} + \left(\frac{\alpha g \Delta z_{N+1/2}}{2} + c_p \right) \overline{w'\theta'}_0 - \frac{\beta g \Delta z_{N+1/2}}{2} \overline{w'S'}_0 - \mathcal{G}_N + \mathcal{G}_1 \quad (26)$$

We check in the following section that this budget is indeed recovered in our SCM code.

5 SCM evaluation and parameterization impacts

In this section, we test on the two idealized cases the sensitivity of the scheme to the formulation of TKE transport, energetic consistency, boundary conditions, mass-flux transport of horizontal momentum, and small plume area assumption. We also quantify energy biases of inconsistent formulations, including double-counting errors due to inconsistent boundary conditions. The constants c_m, c_ϵ, c_k used in the ED terms are the same as the constants used in the TKE equation of the LES model. The parameters used for the plume equations closures have been chosen as $\beta_1 = 0.99, \beta_2 = 1.99, a = 1., b = 1., b' = 0.75, C_u = 0.5, a_p^0 = 0.2, \delta_0 = 1.125$. A careful tuning and uncertainty quantification of the parameters, using for instance statistical method (e.g. Souza et al., 2020; Couvreux et al., 2021), is left for future studies. Sensitivity to time step and number of levels is presented in Appendix D.

5.1 Impact of the energetic consistency and comparison to EVD

5.1.1 Bulk production

In this section, we evaluate three different configurations of the SCM against LES data. First, an EDMF scheme in which an ED parameterization of the TKE equation is used (referred to as "EDMF-inconsistent"), namely

$$\partial_t k + \partial_z(-K_k \partial_z k) = -K_\phi \partial_z \overline{b} + K_u (\partial_z \overline{\boldsymbol{u}}_h)^2 - \overline{\epsilon} \tag{27}$$

This configuration is not energetically consistent since the contributions of MF to the buoyancy and shear production of TKE are missing (Part I). It would be the result of an independent coupling of TKE and MF schemes. The second configuration consists of the previously detailed EDMF scheme in which the TKE equation consistently includes the contribution of MF terms to energy transfers (referred to as "EDMF-Energy") as detailed in (2). Finally, an ED closure based on a TKE-scheme, along with enhanced vertical diffusivity to $10\,\mathrm{m^2 s^{-1}}$ at depths where $N^2 < 0$ is tested and implemented for reference. This is the standard option in NEMO (Madec et al., 2019), and we will refer to it as "ED+EVD". The comparison of the three aforementioned configurations are plotted for the two LES cases on figures 6 and 7. ED+EVD necessarily produce unstable (near-neutral) temperature profiles (fig. 6(a) and 7(a)) when the associated temperature flux is positive, since by design ED+EVD can only allow down-gradient fluxes. Moreover ED+EVD fails to reproduce the correct magnitude of the so-called vertical entrainment zone (e.g. Garcia & Mellado, 2014), in which penetrative convection generates negative temperature flux and sharpens the temperature gradients at the base of the mixed layer. The lack of penetrative convection is known to reduce the deepening rate (e.g. chap. 6, Garratt, 1994), thus producing an important bias of a hundred meters regarding the mixed layer depth compared to LES. However in this region the negative flux of temperature could have been represented by an ED-only closure, since positive gradient of temperature are expected (e.g. (Bretherton & Park, 2009)) ; the observed bias of the entrainment flux is not due to the usage of an ED closure, but to the detailed formulation of such a downgradient scheme. On the other hand, EDMF-inconsistent and EDMF-energy equally perform in representing these profiles. The absence of a noticeable effect of the energetic consistency on the temperature mean and flux profiles is a consequence of the small value of the eddy-diffusivity fluxes (dashed lines) in the mixed layer. When considering the TKE profile (fig. 6(c) and 7(c)), ED+EVD can model the correct order of magnitude, however, the TKE does not penetrate enough. EDMF-inconsistent fails to reproduce TKE due to energetic inconsistency. Indeed, looking at temperature and velocity fluxes allows us to infer that the losses of resolved energy due to buoyancy and shear are dominated by the MF contributions. However, such contributions are not included as sources of TKE for the EDMF-inconsistent scheme, leading to the very low levels of TKE observed in the simulation. EDMF-energy can reproduce accurate profiles of TKE. The main discrepancies arise close to the surface and at the base of the mixed layer. How-

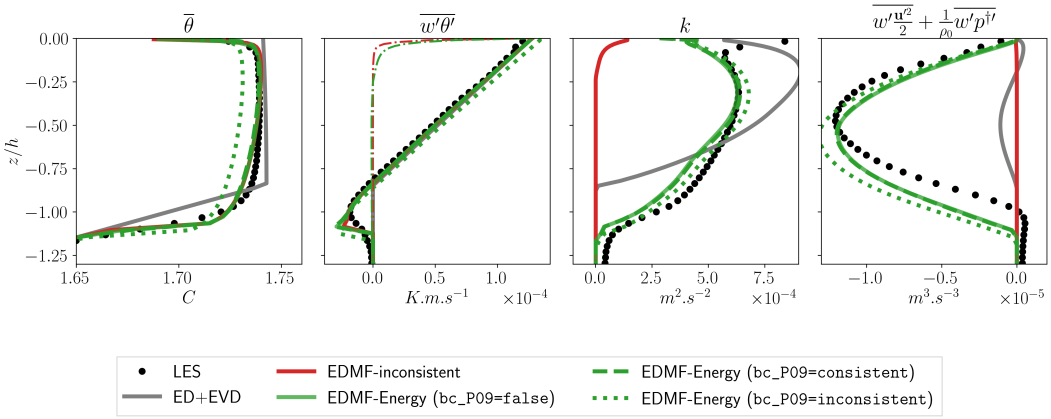

Figure 6: Mean and turbulent profiles for the case FC500 case after $72h$ of simulation. LES data (black dots), ED+EVD scheme (gray line), EDMF-inconsistent (red line), EDMF-energy (green line), EDMF-energy-`bc_P09=consistent` (green dashed) and EDMF-energy-`bc_P09=inconsistent` (green dotted) are represented, along with the ED contribution to the temperature fluxes for EDMF-inconsistent (dashed-dotted red) and EDMF-energy (dash-dotted green).

ever energetic consistency ensures that these discrepancies are only due to modelling choices (such as TKE boundary conditions) and cannot be the result of inconsistent energetics. Regarding the vertical transport of TKE (fig. 6(d) and 7(f)), EDMF-inconsistent is not able to reproduce the LES profile. ED+EVD displays the correct shape, however, the magnitude is approximately ten times less than the reference profile. EDMF-energy accurately reproduces the profile, with a shift downwards of a few percent of the mixed layer depth h.

In Fig. 8, we represent the vertically integrated energy budget of the SCM for the case W005_C500 (FC500 is similar), namely the quantity

$$\int_{-H}^{0} \partial_t \left(E_k + k + E_{i+p}\right) \mathrm{d}z + \left[T_{E_k} + T_k + T_{E_{i+p}}\right]_{z=-H}^{z=0} \tag{28}$$

where the different energy reservoirs and fluxes are presented on equations (2)-(4). As expected, EDMF-energy conserves energy up to round-off errors ($\pm 10^{-12}\mathrm{m}^3\mathrm{s}^{-3}$) whereas EDMF-inconsistent exhibit an energy loss of about $10^{-5}\mathrm{m}^3\mathrm{s}^{-3}$ corresponding to

$$\int_{-H}^{0} \left(-a_p w_p (b_p - \overline{b}) + a_p w_p (\boldsymbol{u}_{h,p} - \overline{\boldsymbol{u}}_h) \cdot \partial_z \overline{\boldsymbol{u}}_h\right) \mathrm{d}z \tag{29}$$

which scales with $B_0 h$.

5.1.2 Boundary conditions

In Part I we showed that inconsistent choices of boundary conditions for plume and mean temperature can lead to energy biases. Here we numerically evaluate the impact of three different plume/mean choices. The default choice for our scheme is

$$(\texttt{bc\_P09=false}) \begin{cases} \theta_p|_0 & = \overline{\theta}|_0 \\ -K_\phi \partial_z \overline{\theta}|_0 & = \overline{w'\theta'}|_0 \end{cases} \tag{30}$$

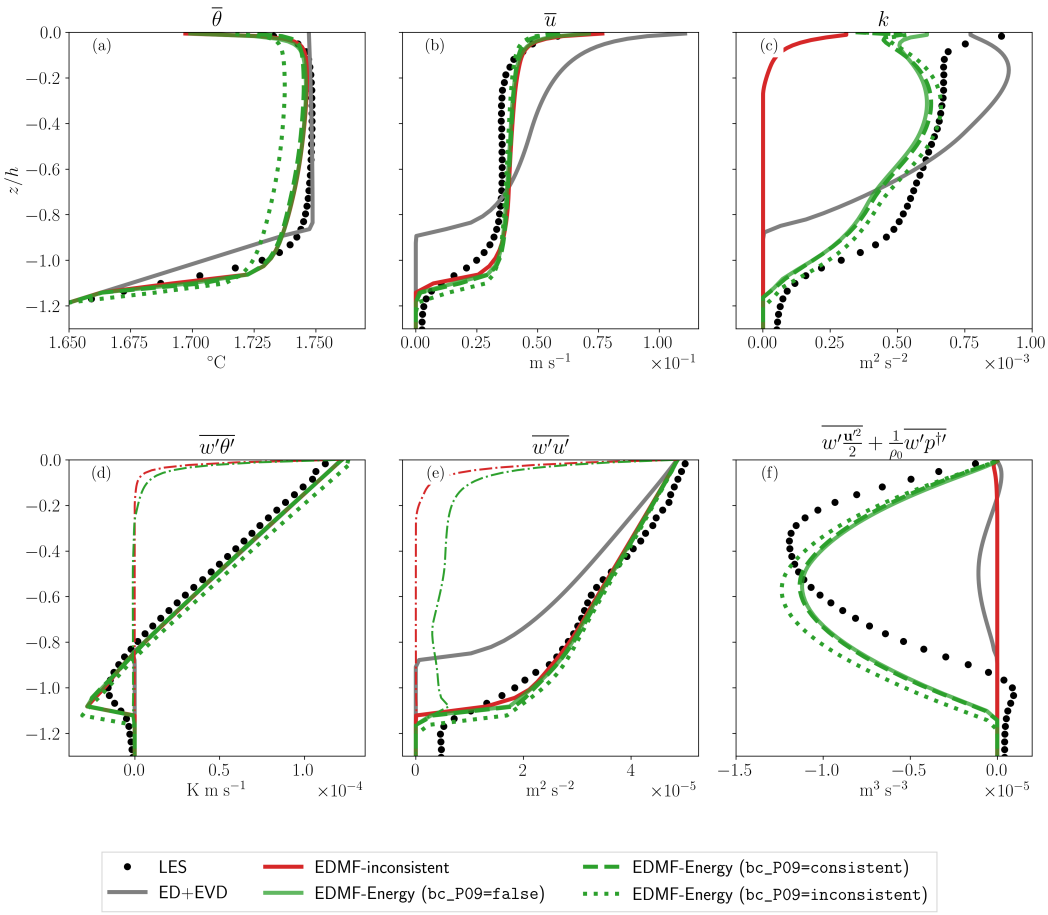

Figure 7: Same as figure 6 for the case W005_C500.

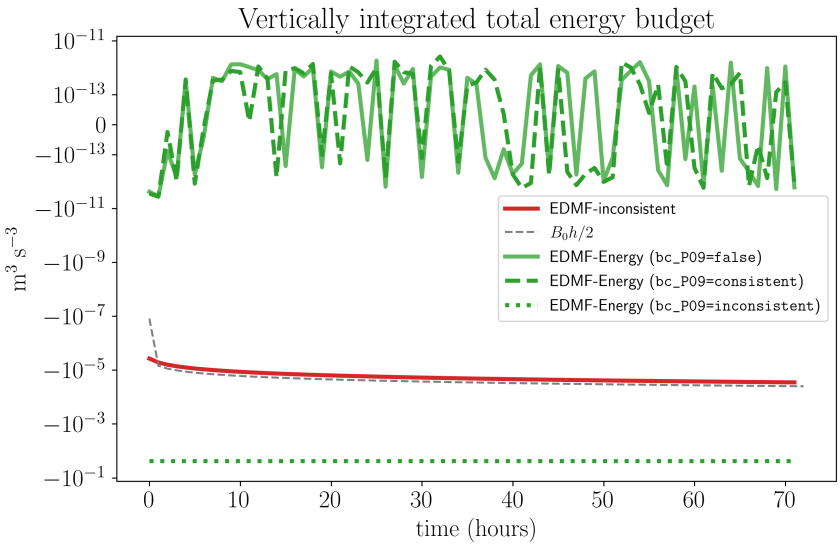

Figure 8: Time series of the vertically integrated energy budget (28) for the case W005_C500 (see text for details).

which result in the physical energy flux $T_{E_{i+p}}|_0 = c_p\overline{w'\theta'}|_0$. The boundary condition proposed in (Pergaud et al., 2009), adapted from (Soares et al., 2004),

$$(\texttt{bc\_P09=inconsistent}) \begin{cases} \theta_p|_0 = \overline{\theta}|_0 + \beta_{\mathrm{P09}} \dfrac{\overline{w'\theta'}|_0}{\sqrt{k}|_0} \\ -K_\phi \partial_z \overline{\theta}|_0 = \overline{w'\theta'}|_0 \end{cases} \tag{31}$$

where $\beta = 0.3$ is a numerical constant. These boundary conditions is equivalent to prescribe the unphysical energy flux $T_{E_{i+p}}|_0 = c_p\overline{w'\theta'}|_0 + c_p\overline{w'\theta'}|_0 \frac{a_p|_0 w_p|_0 \beta_{\mathrm{P09}}}{\sqrt{k}|_0}$ where the second term of the r.h.s. is a spurious source of energy. This bias is due to an inconsistent partitioning of the physical boundary flux $c_p\overline{w'\theta'}|_0$ into ED and MF fluxes. Such bias can be corrected by modifying the ED flux,

$$(\texttt{bc\_P09=consistent}) \begin{cases} \theta_p|_0 = \overline{\theta}|_0 + \beta_{\mathrm{P09}} \dfrac{\overline{w'\theta'}|_0}{\sqrt{k}|_0} \\ -K_b|_0 \partial_z \overline{\theta}|_0 = \overline{w'\theta'}|_0 - a_p|_0 w_p|_0 (\theta_p|_0 - \overline{\theta}|_0) = \left(1 - \dfrac{a_p|_0 w_p|_0 \beta_{\mathrm{P09}}}{\sqrt{k}|_0}\right) \overline{w'\theta'}|_0 \end{cases} \tag{32}$$

leading to the physical energy flux $T_{E_{i+p}}|_0 = c_p\overline{w'\theta'}|_0$.

On figures 6 and 7 we expose the result of these different boundary conditions on mean and turbulent quantities after 72h of simulation. For the EDMF-energy scheme, solutions computed using `bc_P09=false` and `bc_P09=consistent` coincide, whereas `bc_P09=inconsistent` exhibit a cool bias of $\simeq 0.01^o C$ on temperature profiles (fig. 6(a) and 7(a)) due to the spurious flux imposed at the surface. Since buoyancy in the mixed layer scales with $N^2 h$ (Garratt, 1994) this bias is expected to increase with the mixed layer depth. Finally it induces bias of a few percents on the TKE and TKE flux profiles. On figure 8 vertically integrated total energy budgets are represented against time for these different boundary conditions for the case W005_C500. "`bc_P09=false`" and "`bc_P09=consistent`" equally performs at conserving energy up to round-off errors ($\pm 10^{-12}\mathrm{m}^3\mathrm{s}^{-3}$), whereas "`bc_P09=inconsistent`" exhibits an important bias of $10^{-1}\mathrm{m}^3\mathrm{s}^{-3}$.

5.2 Impact of TKE transport

In fig. 10 and 9 we compare the new TKE transport parameterization exposed in sec. 2 to a standard ED+EVD formulation, and to the MF closures proposed by (Witek et al., 2011) and by (Han & Bretherton, 2019).

$$\overline{w' \frac{\boldsymbol{u}' \cdot \boldsymbol{u}'}{2}} = \underbrace{-K_k \partial_z k}_{\text{ED}} + \underbrace{\overbrace{a_p w_p (k_p - k)}^{\text{Han \& Bretherton 2019}} + \overbrace{a_p w_p^3}^{\text{Witek et al. 2011}} + \frac{a_p w_p}{2} \|\boldsymbol{u}_{h,p} - \overline{\boldsymbol{u}}_h\|^2}_{\text{new EDMF}} \tag{33}$$

Moreover, note that we use a different plume TKE equation than the one used in Han and Bretherton (2019),

$$a_p w_p \partial_z k_p = \underbrace{\overbrace{E\,(k - k_p)}^{\text{Han \& Bretherton 2019}} + E\left(\frac{1}{2}\|\boldsymbol{u}_p - \overline{\boldsymbol{u}}\|^2\right) - a_p \epsilon_p}_{\text{new EDMF}} \tag{34}$$

The choice of TKE transport seems to have a negligible impact on temperature, temperature fluxes, velocity and momentum fluxes. When looking at TKE fluxes (fig. 9(d) and 10(f)), all parameterizations reproduce the bell-shape but exhibit a consistent shift downwards of approximately $0.1h$. Haghshenas and Mellado (2019b) mention that the local maximum at the base of the mixed layer is caused by shear production of TKE and corresponds to a upwards transport from the mixed layer base into the mixed layer interior. None of the parameterizations are able to capture this effect. Regarding the minimum of the flux, ED+EVD and Han & Bretherton parameterizations result in biases

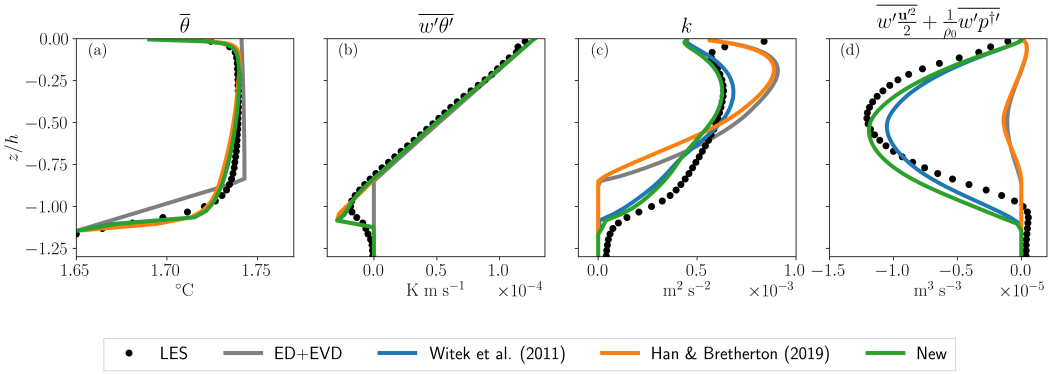

Figure 9: Vertical profiles of (a) temperature, (b) temperature flux, (c) turbulent kinetic energy and (d) turbulent transport of TKE for the FC500 case after $72h$ of simulation. LES data (black dots) are ED+EVD scheme (gray line) represented, as well as three energetically consistent EDMF scheme differing only by their parameterization of TKE transport: Witel et al. 2011 (blue line), Han & Bretherton 2019 (orange line) and the new formulation (green line).

of 90% and 80% biases compared to LES, whereas Witek et al. has the correct value and the new parameterization present a 10% overestimate of the maximum. We will see that this overestimation can be corrected if the assumption of small a_p is relaxed, see sec. 5.3. Transport of TKE has a direct effect on the profile of TKE (fig. 9(c) and 10(c)). The surface production of TKE seems not enough redistributed on the vertical for ED+EVD and Han & Bretherton schemes, leading to insufficient penetration of TKE inside the lower half of the mixed layer. The more realistic TKE transports of Witek et al. and of the new scheme lead to a better penetration of the TKE inside the mixed layer. The surface TKE bias, also present in the free convective case on fig. 6 may be related to boundary condition choices that should be further investigated. Our implementation of Han & Bretherton reproduces well the shape of TKE plotted on their figure 4; but their implementation exhibits a clear lack of production of TKE.

5.3 Impact of horizontal momentum transport and small plume area

In section 3.3, analysis of LES revealed that the assumption $a_p \ll 1$ was not fully satisfied. This small-area assumption can be relaxed with no additional complexity if the subplume fluxes $\overline{w'_p \phi'_p}$ are still neglected. A summary of the EDMF-Energy parameterization in such a regime is presented in Tab. 4. Moreover we examine the impact of the mass-flux on horizontal momentum transport by comparing simulations in which $\overline{w'\boldsymbol{u}'_h}^{MF} = 0$ (a choice made in several studies, e.g Tan et al. (2018); Cohen et al. (2020); Giordani et al. (2020)) to simulations where the horizontal velocity plume model exposed in tab. 1 leads to $\overline{w'\boldsymbol{u}'_h}^{MF} \neq 0$. The cross-comparison of small-area impact and MF horizontal momentum impact leads to four EDMF configurations, presented on fig. 11 for the case W005_C500.

Relaxing the small area assumption mainly affects the minimum of the TKE transport, reducing by 10% which roughly corresponds to the rescaling coefficient $\sigma = 1/(1-a_p)$. As a consequence TKE is less redistributed on the vertical, leading to slightly higher TKE close to the surface and reduced TKE in the interior. Other mean fields and fluxes do not seem affected. However, the influence of the small plume area would be more clearly seen in the gray zone of convection, i.e. when the horizontal size of convective structures approach the horizontal size of the LES domain (Honnert, 2022). For 3D implementa-

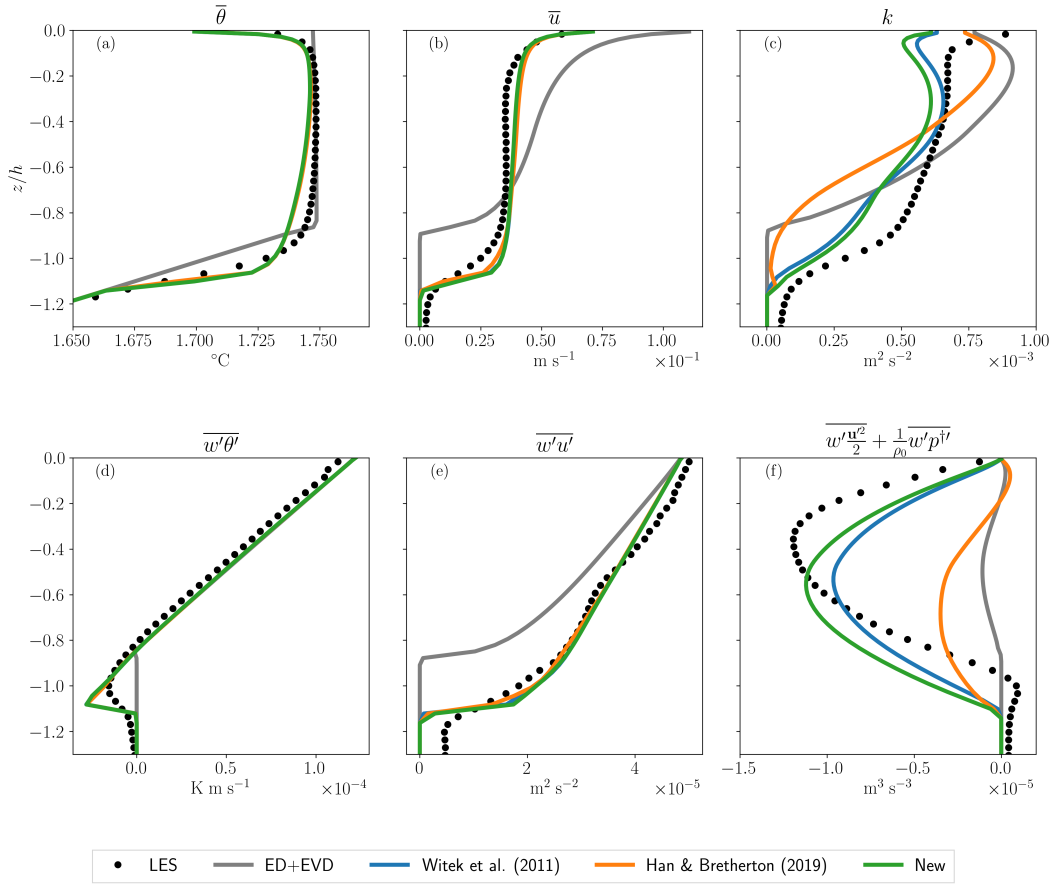

Figure 10: Same as figure 10 for the case W005_C500.

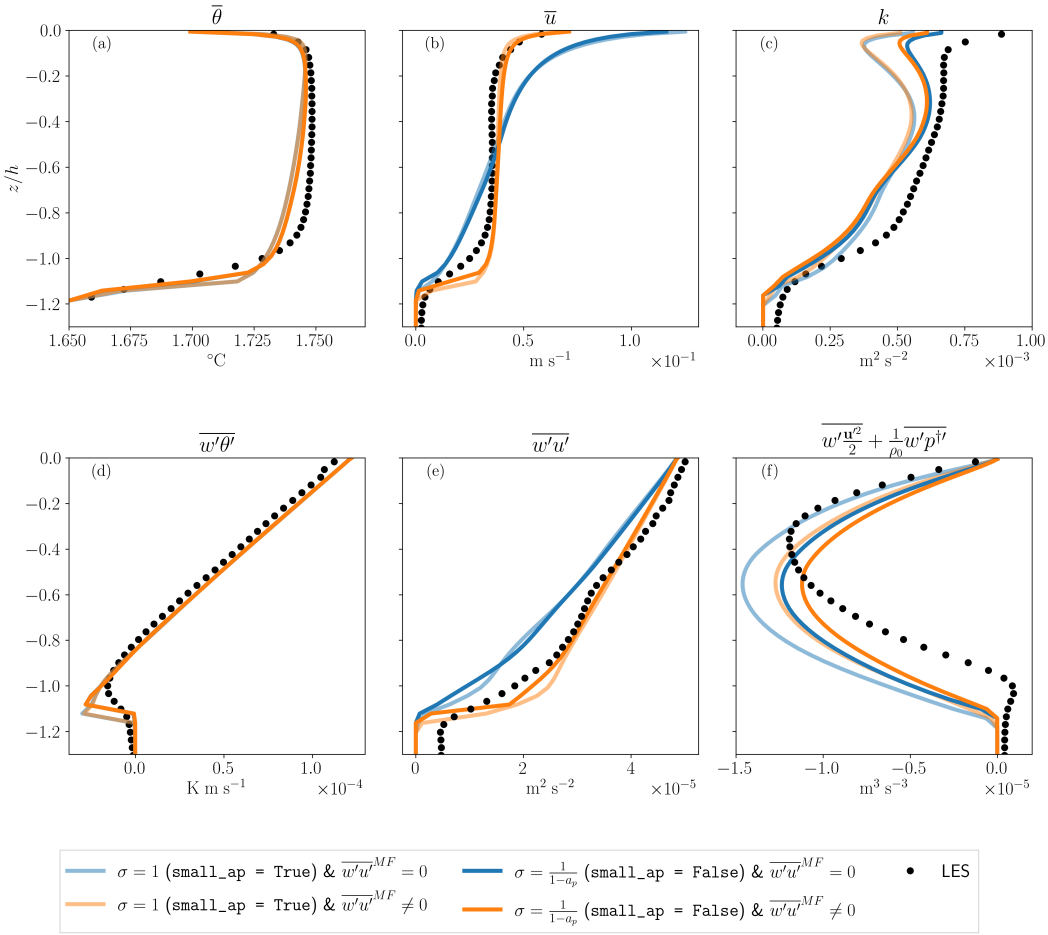

Figure 11: Mean and turbulent profiles for the W005_C500 case after $72h$ of simulation. Different configurations of EDMF-energy are used: small plume area assumption (transparent lines) or not (solid lines); MF on momentum flux (orange lines) or not (blue lines).

tions of the parameterization at resolution lying within the gray zone, the dependency of parameters to resolution should be assessed.

The main effect of MF on horizontal velocities is to increase the momentum flux, which in turn produces more mixing of the zonal velocity compared to the velocities computed with ED-only momentum flux. According to the reference LES the well-mixed profile is more realistic. Configurations with MF momentum flux exhibit more negative minima of TKE flux, which in turn produces higher levels of TKE. However this impact is less important than that of the small-area assumption. This can be explained by the fact that W005_C500 depicts a convection-dominated regime; thus TKE is mainly produced by buoyancy, and the flux of TKE is dominated by the w_p^3 term.

5.4 Realistic case: Hymex/ASICS-MED campaign

We now move to more realistic situations corresponding to a sequence of strong convective events which were documented in the Northwestern Mediterranean during the winter 2013 of the HyMeX/ASICS-MED experiment at the LION buoy. These events corresponds to localized *oceanic deep convection* (Marshall & Schott, 1999) for which the water column is typically mixed over thousands meters, sometime down to the seafloor.

$\sigma = \frac{1}{1-a_p}$	Rescaling coefficient
$\overline{w'\theta'} = \sigma a_p w_p(\theta_p - \overline{\theta}) - K_\phi \partial_z \overline{\theta}$	Vertical turbulent flux of temperature
$\overline{w'S'} = \sigma a_p w_p(S_p - \overline{S}) - K_\phi \partial_z \overline{S}$	Vertical turbulent flux of salt
$\overline{w'\boldsymbol{u}_h'} = \sigma a_p w_p(\boldsymbol{u}_{h,p} - \overline{\boldsymbol{u}}_h) - K_m \partial_z \overline{\boldsymbol{u}}_h$	Vertical turbulent momentum flux
$\partial_z(a_p w_p) = E - D$	Plume area conservation equation
$a_p w_p \partial_z \theta_p = \sigma E(\overline{\theta} - \theta_p)$	Plume temperature equation
$a_p w_p \partial_z S_p = \sigma E(\overline{S} - S_p)$	Plume salinity equation
$a_p w_p \partial_z \boldsymbol{u}_{h,p} = \sigma E(\overline{\boldsymbol{u}}_h - \boldsymbol{u}_{h,p}) + a_p w_p C_u \partial_z \overline{\boldsymbol{u}}_h$	Plume horizontal momentum equation
$a_p w_p \partial_z w_p = -\sigma b E w_p + a_p \left[a B_p + \sigma \frac{b'}{h}(w_p)^2 \right]$	Plume vertical velocity equation
$B_p = b_{\text{eos}}(\theta_p, S_p) - b_{\text{eos}}(\overline{\theta}, \overline{S})$	Buoyancy forcing term
$a_p w_p \partial_z k_p = \sigma E \left((k - k_p) + (1 + a_p^2 \tilde{\sigma}) \frac{1}{2} \lVert \boldsymbol{u}_p - \boldsymbol{u} \rVert^2 \right) - a_p \epsilon_p$	Plume related TKE
$E = a_p C_\epsilon \max(0, \partial_z w_p)$	Lateral entrainment closure
$D = -a_p C_\delta \min(0, \partial_z w_p) - a_p w_p \delta_0 \frac{1}{h}$	Lateral detrainment closure
$\partial_t k - \partial_z (K_k \partial_z k) = K_m (\partial_z \overline{\boldsymbol{u}}_h)^2 - K_\phi \partial_z \overline{b}$	ED related TKE production terms
$-\sigma a_p w_p \left((\boldsymbol{u}_{h,p} - \overline{\boldsymbol{u}}_h) \cdot \partial_z \overline{\boldsymbol{u}}_h - (b_p - \overline{b}) \right)$	MF related TKE production terms
$-\partial_z \left(\sigma a_p w_p \left[k_p - k + \frac{1}{2} \lVert \boldsymbol{u}_p - \boldsymbol{u} \rVert^2 \right] \right)$	MF related TKE transport term
$-\overline{\epsilon}$	TKE dissipation

Table 4: Summary of the plume equations without the small plume area assumption, i.e. without assuming $a_p \ll 1$. Small-area assumption is recovered by imposing $\sigma = 1$ and $\tilde{\sigma} = 0$.

These winter events are common in the Mediterranean sea as well as in the Labrador and Greenland seas, and are of great importance for deep water formation and their overall influence on basin scale dynamics. The ASICS-MED experiment was also used in Giordani et al. (2020) and we use a similar setup here (similar vertical grid as well as similar initial and surface boundary conditions). The experiments are performed with a SCM similar to (1) but including additional Coriolis and solar penetration (using a standard Jerlov law) terms. We use a nonlinear equation of state. We also include penalization terms in the SCM nudging w_p to zero at the ocean floor to account for the effect of the bottom (which is at a depth of 2400 m at the LION buoy). Thanks to the penalization term a no-slip boundary condition is imposed at the bottom and a no-gradient condition is imposed for tracers. The vertical grid resolution ranges from 1 m near the surface to 150 m near the bottom located at $z = -2400$ m. Parameters of the TKE scheme are set to the standard NEMO values, $\boldsymbol{c} = (c_m, c_\epsilon, c_k) = (0.1, \frac{\sqrt{2}}{2}, 0.1)$.

A series of 30-days numerical simulations were carried out starting from January 15, 2013. The surface boundary conditions are shown in Fig. 12. In particular, very strong cooling events occurred during the period of interest. Two simulations were made systematically with an eddy-diffusivity term activated. A first simulation was done with Enhanced Vertical Diffusion (referred to as ED+EVD) which is the standard practice for climate simulations using NEMO, a second one using a mass flux scheme on tracers, dynamics, and with the additional terms for energetic consistency in the TKE equation (referred to as EDMF-energy). To get a more concrete idea of the improvements brought about by the mass flux scheme over the usual practice for NEMO applications (ED+EVD), we show in Fig. 12 (bottom panel) the temporal evolution of the mixed layer depth h_{mxl} computed from mooring data and single-column numerical simulations. h_{mxl} is defined as the depth where the following criterion is met

$$\int_{h_{\mathrm{mxl}}}^{z_{\mathrm{ref}}} \partial_z b_{\mathrm{eos}}(\theta, S = 38.5 \text{ psu})\, dz = \frac{g}{\rho_0}\rho_c \tag{35}$$

with $z_{\mathrm{ref}} = 300$ m and $\rho_c = 0.01$ kg m^{-3}. This choice of reference level is consistent with the one used in Houpert et al. (2016) also with LION buoy observational data. Moreover, the mixed layer depths obtained by applying (35) on the data (see red curve in Fig. 12) are directly comparable with the ones shown in Waldman et al. (2017) (see their Fig. 4). We had to consider a constant salinity in the buoyancy calculation because the salinity data from the LION buoy are noisy in the vertical and did not allow for a robust diagnostic.The bottom panel in Fig. 12 illustrates the fact that the mixed layer depth is significantly better represented by the EDMF-Energy scheme than by the ED+EVD approach. Moreover, a direct comparison with temperature and salinity from mooring data is shown in Fig. 13 at different times. In particular several phases can be identified during the experiment (e.g. Coppola et al., 2017; Waldman et al., 2017): (*i*) in the period 15-25 January 2013 winter convection starts to deepen the mixed layer down to around -800 m to the point of eroding the Levantine intermediate waters (Estournel et al., 2016) (*ii*) in the period 26–29 January 2013 the mixed layer keeps thickening to the depth of the western Mediterranean deep water (≈ -1250 m) (*iii*) in the period 4-9 February 2013 a new intense convective event associated with a strong Mistral event contributes to deepen the mixed layer down to the bottom (reached in 9 February). This is followed by a restratification phase involving horizontal processes that cannot be represented in our SCM formalism which explains why we do not analyze solutions beyond February 9.

6 Discussion and conclusion

In this work, we used idealized Large Eddy Simulations of oceanic convection to analyze hypotheses and outputs of a novel Eddy-Diffusivity Mass-Flux parameterization in a Single-Column Model configuration, derived in Part I (Perrot et al., 2024). This energetically consistent parameterization is rather simple to implement, whether in a code

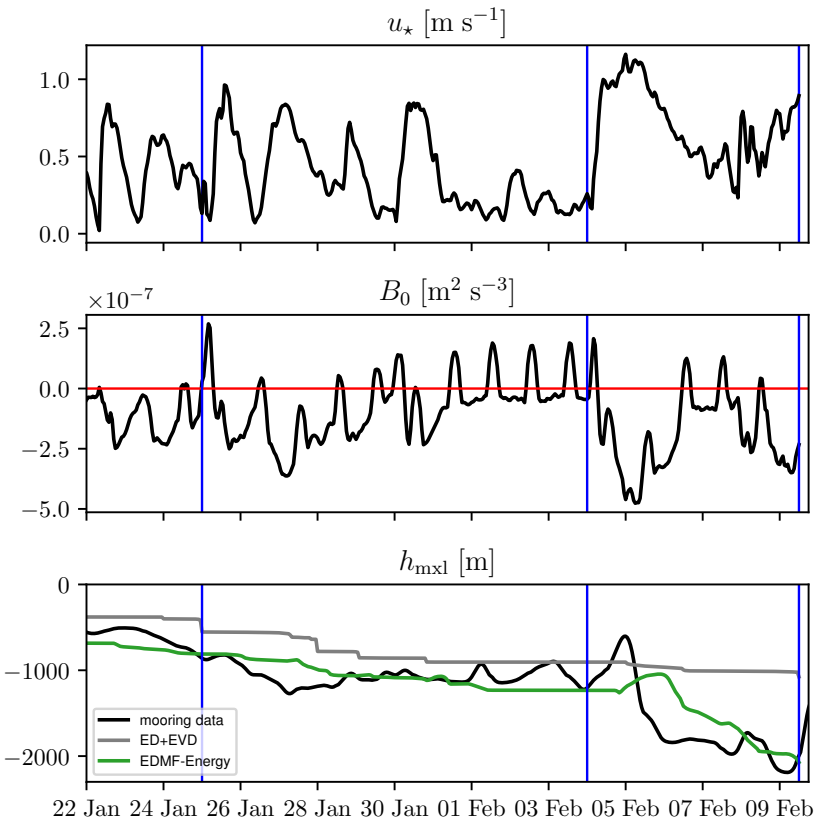

Figure 12: Time series of the friction velocity $u_\star$ (m s^{-1}, top panel) and surface buoyancy flux B_0 (m^2 s^{-3}, middle panel) computed from atmospheric forcings. Time series of mixed layer depth h_{mxl} (m, bottom panel) obtained from observations at the LION buoy (black line) and from single column numerical experiments using ED+EVD (solid gray line) and EDMF-Energy (solid green line). The vertical blue lines correspond to the dates at which the vertical temperature and salinity profiles derived from observations and numerical simulations are compared in Fig. 13.

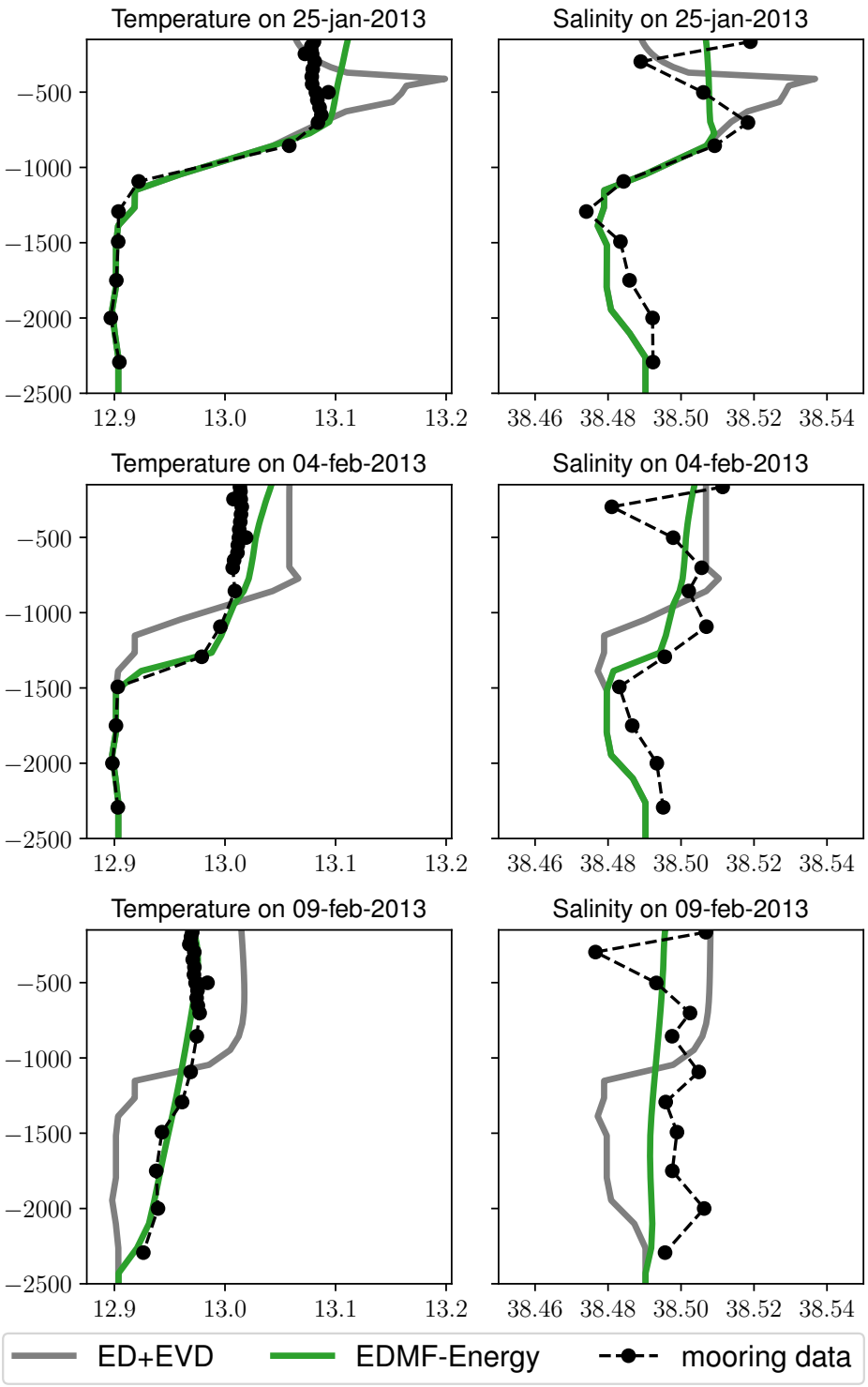

Figure 13: Temperature (^{o}C, left panels) and salinity (psu, right panels) profiles obtained from single column experiments at the location of the LION buoy using an eddy-diffusivity closure with enhanced vertical diffusion (ED+EVD, solid gray lines) and energetically-consistent EDMF (EDMF-Energy, solid green lines). Results from numerical experiments are compared to observations from the LION buoy (dashed black lines) for 4 dates represented on the Fig. 12 by vertical blue lines.

with an existing "non-energetically consistent" EDMF scheme or, more generally, in any code relying on a prognostic TKE equation. The MF terms are obtained by solving a straightforward system of ODEs and take the form of vertical advection terms in the mean equations (see Appendix C for practical details). The proposed approach can also be applied in the case where the ED closure does not use TKE. In this case, it would require to add a prognostic or diagnostic TKE equation (even if it does not interact with the ED term) to enforce energetic consistency.

Using vertical-velocity based conditional sampling of LES, we found that stationarity of the mean convective plume is well satisfied. However even if plume typical radius is small compared to the size of the horizontal domain, plumes typically cover 15 % to 20% of the horizontal domain. Consequently, the assumption of small plume area can be criticized, and we provided and implemented a set of equations without such an hypothesis. Based on LES we also proposed a new EDMF closure for the turbulent transport of TKE which generalizes two existing approaches. We expose the subtleties of numerical implementation of the SCM, including fully consistent discrete energy budgets based on their continuous counterparts. This study highlights how energy considerations can unambiguously guide discretizations. Finally we performed a series of sensitivity experiment to different modelling aspects regarding energetic consistency, boundary conditions, transport of TKE, transport of horizontal momentum by MF and small plume area assumption. Temperature and flux of temperature profiles do not appear to significantly be affected by such choices, and the SCM reproduces LES profiles compared to EVD. Modelling plume horizontal velocities distinct from the mean seems necessary to properly reproduce horizontal velocities and its fluxes. The usage of an energetically consistent TKE equation and along with the new formulation of TKE transport is key to obtaining realistic TKE and turbulent transport of TKE profiles. We also quantify the energy loss of inconsistent formulations, due to either inconsistent TKE equation or inconsistent boundary conditions. Surprisingly, removing the assumption of small plume area only affects the transport of TKE. All these findings are based on idealized cases, where in particular ED fluxes are small explaining the negligible retroaction of energetic consistency and TKE on the solutions. Thus a further assessment of global 3D simulations is a necessary next step to understand the implications of energetic consistency. To further illustrate that the MF concept is a credible alternative to the traditional approaches used in the oceanic context (using e.g. an enhanced vertical diffusion) the proposed scheme is validated in a single-column configuration against observational data of oceanic convection from the LION buoy.

To implement and then assess the impact of this energetically consistent parameterization on realistic 3D oceanic simulations a calibration of the remaining "free" parameters must be achieved (Hourdin et al., 2017; Couvreux et al., 2021). It should be performed on parameters whose universality can sometimes be statistically assessed (Souza et al., 2020), and should be mathematically and physically constrained as much as possible. We believe that designing energetically consistent parameterization is a way to achieve more realistic models before their tuning.

Appendix A Mixing length and dissipation computations

For the oceanic applications detailed in this article, we have chosen a formulation of eddy-diffusivity and viscosity close to that used in the NEMO ocean model (Madec et al., 2019). The eddy-viscosity and diffusivity are classically assumed to be related to TKE by

$$\begin{aligned} K_u &= c_m l_m \sqrt{k} \\ K_\phi &= K_u (\mathrm{Pr}_t)^{-1} \end{aligned}$$

with l_m a mixing length scale, Pr_t the non-dimensional turbulent Prandtl number, and c_m is a constant ($c_m = 0.1$ in NEMO). The mixing length l_m is calculated in two steps

by considering separately the length scales $l_{\rm up}$ and $l_{\rm dwn}$ associated respectively to upward and downward movements : (1) $l_{\rm up}$ and $l_{\rm dwn}$ are initialized assuming $l_{\rm up} = l_{\rm dwn} = \sqrt{2k}\tau_{\rm ed}$ with $\tau_{\rm ed}$ a characteristic time equal to $1/N = (\partial_z \overline{b})^{-1}$ (2) a physical limitation is used to guarantee that $l_{\rm up}$ and $l_{\rm dwn}$ do not exceed the distance to the top and the bottom, this limitation amounts to controlling the vertical gradients of $l_{\rm up}$ and $l_{\rm dwn}$ such that they are not larger that the variations of depth (*e.g.* Madec et al., 2019). Once $l_{\rm up}$ and $l_{\rm dwn}$ are computed the mixing length is taken as $l_m = \min(l_{\rm up}, l_{\rm dwn})$. The turbulent Prandtl number is modelled by $\Pr_t = \min(\Pr_t^{\max}, \max({\rm Ri}/{\rm Ri}_c, 1))$ with ${\rm Ri} = N^2/\|\partial_z \overline{\mathbf{u}}_h\|^2$, $\Pr_t^{\max} = 10$ and ${\rm Ri}_c = 0.2$.
The viscous dissipation is parameterized as $\overline{\epsilon} = \frac{c_\epsilon}{l_\epsilon} k^{3/2}$, where $c_\epsilon = \sqrt{2}/2$ is a numerical constant and the dissipation length is $l_\epsilon = \sqrt{l_{\rm up} l_{\rm dwn}}$ (e.g. Gaspar et al., 1990).

Appendix B Third Order Moment computations

By definition we have

$$k = \overbrace{\frac{1}{2}a_e\|\boldsymbol{u}_e - \overline{\boldsymbol{u}}\|^2 + a_e k_e}^{a_e k_e^t} + \overbrace{\frac{1}{2}a_p\|\boldsymbol{u}_p - \overline{\boldsymbol{u}}\|^2 + a_p k_p}^{a_p k_p^t} \tag{B1}$$

$$\implies k_p^t - k_e^t = \frac{1}{1-a_p}(k_p^t - k) \tag{B2}$$

thus

$$\begin{aligned}
{\rm III}_e + {\rm III}_p + {\rm IV}_e + {\rm IV}_p &= a_p w_p \left(k_p + \frac{1}{2}\|\boldsymbol{u}_p - \overline{\boldsymbol{u}}\|^2\right) + a_e w_e \left(k_e + \frac{1}{2}\|\boldsymbol{u}_e - \overline{\boldsymbol{u}}\|^2\right) && \text{(B3)}\\
&= a_p w_p \left(k_p + \frac{1}{2}\|\boldsymbol{u}_p - \overline{\boldsymbol{u}}\|^2 - k_e - \frac{1}{2}\|\boldsymbol{u}_e - \overline{\boldsymbol{u}}\|^2\right) && \text{(B4)}\\
&= a_p w_p \left(k_p^t - k_e^t\right) && \text{(B5)}\\
&= \frac{a_p}{1-a_p} w_p (k_p^t - k) && \text{(B6)}
\end{aligned}$$

Appendix C Discretization of mass-flux equations

We start from the standard grid arrangement used in oceanic models which are usually discretized on a Lorenz grid in the vertical (density is located in the center of the cells on the vertical). We consider N grid cells in the vertical with thickness $\Delta z_j = z_{j+1/2} - z_{j-1/2}$ ($z_{1/2} = -H$ and $z_{N+1/2} = 0$ the surface) such that $\sum_{j=1}^{N} \Delta z_j = -H$. For the discrete values, not to interfere with the grid indices, the subscript p for the plume quantities is now a superscript such that plume quantities are now noted $X^p_{j+1/2} = X_p(z = z_{j+1/2})$. In the following, we consider that the plume quantities and k are discretized at cell interfaces and the mean quantities $\overline{X}$ are discretized at cell centers and are interpreted in a finite-volume sense (i.e. $\overline{X}_j = \dfrac{1}{\Delta z_j}\displaystyle\int_{z_{j-1/2}}^{z_{j+1/2}} \overline{X}(z)\ {\rm d}z$). We start from the mass-flux equations given in Tab. 1 with $\widetilde{b}' = b'/h$ but in conservative form (except for the vertical velocity and TKE plume equations) :

$$\partial_z(a_p w_p) = E - D \tag{C1}$$

$$\partial_z(a_p w_p \phi_p) = E\overline{\phi} - D\phi_p \tag{C2}$$

$$\partial_z(a_p w_p \boldsymbol{U}_p) = E\overline{\boldsymbol{U}} - D\boldsymbol{U}_p \tag{C3}$$

$$w_p \partial_z w_p = -(E/a_p)(b w_p) + a B_p + \widetilde{b}' w_p^2 \tag{C4}$$

$$a_p w_p \partial_z k_p = E\left(k - k_p + \frac{1}{2}(\overline{\boldsymbol{u}}_p - \overline{\boldsymbol{u}})^2\right) - a_p(\epsilon_\nu)_p \tag{C5}$$

where the equation for horizontal momentum has been manipulated to have the same form as the ϕ_p equation by taking $\boldsymbol{U}_p = \boldsymbol{u}_{h,p} - C_u\overline{\boldsymbol{u}}_h$ and $\overline{\boldsymbol{U}} = (1-C_u)\overline{\boldsymbol{u}}_h$. The advective form is used for the w_p equation to make the computation of w_p independent of a_p (with the closure hypothesis given in Tab. 4 for E, E/a_p is independent of a_p); the motivations for this will become clearer later. The mass-flux equations correspond to a first-order nonlinear set of ODEs. There are a whole lot of methods for solving such initial value problems. We present here a simple method combining explicit (Euler) and semi-implicit (Crank-Nicolson) steps as the use of more advanced methods did not produce significantly different results. In the following, we describe the different steps for the resolution starting from known initial values $X^p_{N+1/2}$ at the surface and advancing downward.

C1 Initial conditions

The discrete form of the boundary conditions given in eq. (30) are obtained by a linear extrapolation of $\overline{\phi}_N$ and $(\overline{\boldsymbol{u}}_h)_N$ toward the surface.

$$\begin{aligned} w^p_{N+1/2} &= -w^p_{\min} \\ \phi^p_{N+1/2} &= \frac{(2\Delta z_N + \Delta z_{N-1})\overline{\phi}_N - \Delta z_N \overline{\phi}_{N-1}}{\Delta z_N + \Delta z_{N-1}} \\ \boldsymbol{U}^p_{N+1/2} &= (1-C_u)\frac{(2\Delta z_N + \Delta z_{N-1})(\overline{\boldsymbol{u}}_h)_N - \Delta z_N(\overline{\boldsymbol{u}}_h)_{N-1}}{\Delta z_N + \Delta z_{N-1}} \end{aligned} \tag{C6}$$

Since the TKE k is already discretized at cell interfaces the boundary condition for k_p does not require an extrapolation. In particular the condition on ϕ_p leads to the following value of the B_p term in the topmost grid cell :

$$B^p_N = \Delta z_N \left(\frac{\overline{b}_N - \overline{b}_{N-1}}{\Delta z_N + \Delta z_{N-1}}\right) = \frac{\Delta z_N}{2}\left(N^2\right)_{N-1/2}$$

meaning that using the condition (C6) allows to trigger convection as soon as the Brunt-Väisälä frequency is negative. Indeed a negative value of B^p_N in the RHS of the w_p-equation (C4) leads to a positive value of $(\partial_z w_p)_N$ and thus larger negative values of w_p when going downward.

C2 w_p-equation and mixed layer depth

The w_p-equation (C4) using the entrainment E given in Tab. 4 can be formulated as

$$\partial_z w_p^2 + b\beta_1 \min(\partial_z w_p^2, 0) = 2aB_p + 2\widetilde{b}' w_p^2$$

which can be discretized in a straightforward way as

$$\begin{aligned} \widetilde{\beta}\left[(w^p)^2_{j+1/2} - (w^p)^2_{j-1/2}\right] &= 2a\Delta z_j B^p_j + (\widetilde{b}'\Delta z_j)\left[(w^p)^2_{j+1/2} + (w^p)^2_{j-1/2}\right] \\ B^p_j &= b_{\text{eos}}(\phi^p_{j+1/2}) - b_{\text{eos}}(\overline{\phi}_j) \end{aligned} \tag{C7}$$

where $\widetilde{\beta} = 1 + b\beta_1$ if $aB^p_j + \widetilde{b}'(w^p)^2_{j+1/2}$ is negative and $\widetilde{\beta} = 1$ otherwise. Knowing $w^p_{j+1/2}$, it is easily found that

$$(w^p)^2_{j-1/2} = \frac{(\widetilde{\beta} - \widetilde{b}'\Delta z_j)(w^p)^2_{j+1/2} - 2a\Delta z_j B^p_j}{\widetilde{\beta} + \widetilde{b}'\Delta z_j} \tag{C8}$$

Once this quantity falls below a certain threshold $(w^p_{\min})^2$, the plume is considered evanescent. In the oceanic context we consider $w^p_{j-1/2} = -\sqrt{(w^p)^2_{j-1/2}}$ for the rest of the calculations to guarantee that $w^p_{j-1/2}$ is strictly negative. The upwinding used to compute

B_p in (C7) in addition to the fact that the w_p-equation does not depend on a_p avoid the need for an iterative process to solve the mass-flux equations.

The mixed layer depth h we consider to scale the parameter b' is the depth at which the discrete value of w^p equals $w^p_{\min}$. In practice, as soon as $(w^p)^2_{j-1/2}$ given by (C8) is smaller than $(w^p_{\min})^2$ we use (C8) to compute the distance $\Delta z^\star_j$ below $z_{j+1/2}$ where the plume vertical velocity exactly equals $w^p_{\min}$:

$$\Delta z^\star_j = \frac{(w^p)^2_{j+1/2} - (w^p_{\min})^2}{2aB^p_j + \widetilde{b}'\left((w^p)^2_{j+1/2} + (w^p_{\min})^2\right)}$$

leading to $h = z_{j+1/2} - \Delta z^\star_j$. To compute $\Delta z^\star_j$ we assume that $\widetilde{\beta} = 1$ because the bottom of the plume is reached only if we are in the detrainment zone.

C3 Continuity and tracer equations

The entrainment E_j and detrainment D_j rates given in Tab. 4 (taken from Rio et al. (2010)) discretized on a grid cell j correspond to

$$\begin{aligned}
\Delta z_j E_j &= \frac{1}{2}\left(a^p_{j+1/2} + a^p_{j-1/2}\right)\beta_1(\delta_z w^p)^+_j \\
\Delta z_j D_j &= \frac{1}{2}\left(a^p_{j+1/2} + a^p_{j-1/2}\right)\left[-\beta_2(\delta_z w^p)^-_j - \frac{\delta_0 \Delta z_j}{2}(w^p_{j+1/2} + w^p_{j-1/2})\right]
\end{aligned}$$

where $(\delta_z w^p)^+_j = \max\left(w^p_{j+1/2} - w^p_{j-1/2}, 0\right)$ and $(\delta_z w^p)^-_j = \min\left(w^p_{j+1/2} - w^p_{j-1/2}, 0\right)$. Integrating from $z_{j-1/2}$ to $z_{j+1/2}$ the continuity equation and ϕ_p equations we obtain

$$\begin{aligned}
(a^p w^p)_{j+1/2} - (a^p w^p)_{j-1/2} &= \Delta z_j (E_j - D_j) \\
(a^p w^p \phi^p)_{j+1/2} - (a^p w^p \phi^p)_{j-1/2} &= \Delta z_j E_j \overline{\phi}_j - (\Delta z_j D_j/2)\left(\phi^p_{j+1/2} + \phi^p_{j-1/2}\right)
\end{aligned}$$

which can also be extended to the horizontal momentum equation formulated using $\boldsymbol{U}_p$. Since at this stage $w^p_{j+1/2}$ and $w^p_{j-1/2}$ are known, the continuity equation is used to compute $a^p_{j-1/2}$ through

$$\begin{aligned}
a^p_{j-1/2} &= a^p_{j+1/2}\left\{\frac{2w^p_{j+1/2} - \mathrm{EmD}_j}{2w^p_{j-1/2} + \mathrm{EmD}_j}\right\} \\
\mathrm{EmD}_j &= \beta_1(\delta_z w^p)^+_j + \beta_2(\delta_z w^p)^-_j + \min\left\{\frac{\delta_0 \Delta z_j}{2}(w^p_{j+1/2} + w^p_{j-1/2}), -2(w^p_{\min})\right\}
\end{aligned} \tag{C9}$$

Note that a_p is subject to a boundedness requirement as $0 \leq a_p \leq 1$. Assuming $0 \leq a^p_{j+1/2} \leq 1$, sufficient conditions to guarantee that $a^p_{j-1/2} \leq 1$ are $\beta_1 \leq 1$ and $\beta_2 \geq 1$ and a sufficient condition to guarantee that $a^p_{j-1/2} \geq 0$ is $\beta_2 < 2$. Moreover a constraint is added on the background detrainment δ_0 in (C9) to guarantee that $a^p_{j-1/2} = 0$ as soon as $w^p_{j+1/2} = w^p_{j-1/2} = -w^p_{\min}$ which occurs once outside the plume.

Once $a^p_{j-1/2}$ is known, it is possible to compute $\phi^p_{j-1/2}$ (as well as $\boldsymbol{U}^p_{j-1/2}$). The proposed discretization ensures that the compatibility between the continuity and the tracer equations is maintained at the discrete level (*i.e.* we recover the continuity equation for $\phi^p_{j+1/2} = \phi^p_{j-1/2} = 1$ and $\overline{\phi}_j = 1$).

The same reasoning can be applied to solve the k_p equation, which presents no additional difficulties as all necessary quantities $w^p_{j\pm1/2}$, $a^p_{j\pm1/2}$ and $\boldsymbol{u}^p_{j\pm1/2}$ are known.

In summary, the proposed discretization guarantees that w_p is strictly negative, that a_p is bounded between 0 and 1, and that the continuity and tracer equations are compatible, without the need for an iterative solution procedure.

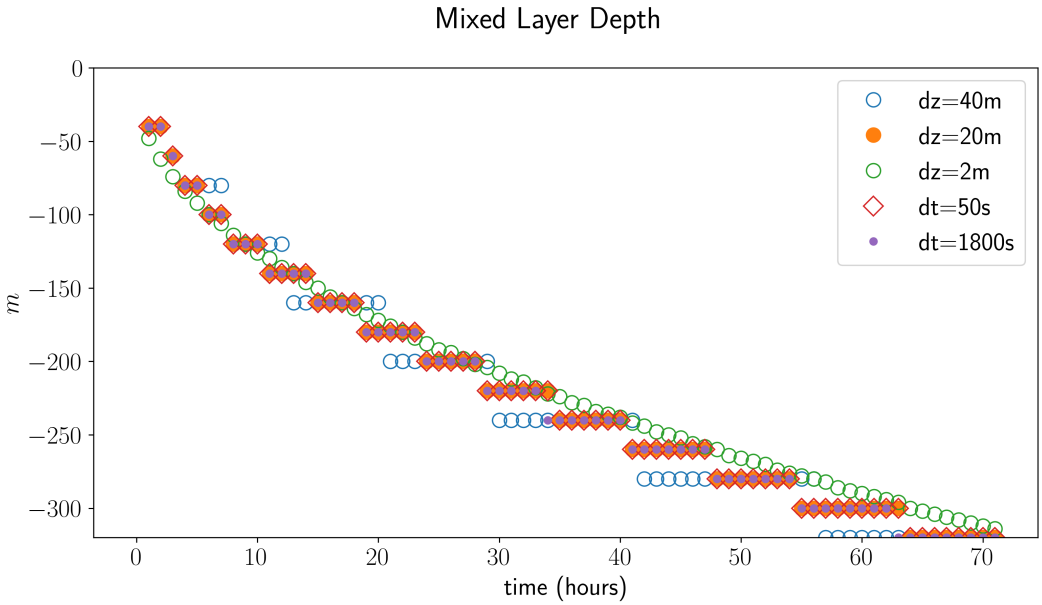

Figure D1: Mixed layer depth (MLD) computed as the minimum of temperature flux for different time steps (dt) and number of levels (nz), LES data and analytical expression.

Appendix D Time step and vertical resolution sensitivity

On figure D1 we expose mixed layer depth (MLD) sensitivity to time step and vertical resolution for the case W005_C500. During deep convection, the mixed layer can reach depths at which vertical grid spacing is important, justifying the relevance of large vertical resolution such as $dz = 40m$.

Open Research

Data Availability Statement

Data from the Lion mooring (located in the Gulf of Lion; Mediterranean sea) are freely accessible from Bosse et al. (2023). The output from LES simulations and the initial and surface boundary conditions for the Hymex/ASICS-MED experiments are available at the Zenodo archive https://zenodo.org/records/10619442.

Software Availability Statement

The LES model Méso-NH can be downloaded at http://mesonh.aero.obs-mip.fr/mesonh57. All the SCM codes used in this study have been made available and can be found at the Zenodo archive https://zenodo.org/records/10619442. It includes the single-column model with Eddy-Diffusivity Mass-Flux turbulent closure developed from scratch. The latter consists of low-level code written in Fortran interfaced with Python using F2PY (Peterson, 2009). The single-column simulations analyzed in this study can be executed from a high-level Python driver code without any intervention on the Fortran code. The high-level Python driver code and scripts to reproduce the figures are available in the Zenodo archive. The Fortran code contains inline documentation following the FORD (Fortran Documenter) format.

Acknowledgments

The authors would like to thank Hilary Weller and two anonymous reviewers for their constructive comments to help improve our manuscript. This work was supported by the *institut des Mathématiques pour la Planète Terre* (iMPT) through the project "Coherent sub-grid scale modeling for ocean climate models". This study was carried out as part of the technological defense project PROTEVS2 under the auspices of the French Ministry of the Armies / DGA, was funded in part by l'Agence Nationale de la Recherche (ANR), project ANR-23-CE01-0009. MP was supported by a PhD fellowship from Ecole Normale Supérieure Paris. The authors are extremely grateful to Jean-Luc Redelsperger for his essential contributions to the MESO-NH model.

References

Bosse, A., Testor, P., Coppola, L., Bretel, P., Dausse, D., Durrieu de Madron, X., ... D'ortenzio, F. (2023). *LION observatory data.* Retrieved from `https://doi.org/10.17882/44411` (Type: Dataset) doi: 10.17882/44411

Bretherton, C. S., & Park, S. (2009, June). A New Moist Turbulence Parameterization in the Community Atmosphere Model. *Journal of Climate*, *22*(12), 3422–3448. Retrieved 2024-07-03, from `https://journals.ametsoc.org/view/journals/clim/22/12/2008jcli2556.1.xml` (Publisher: American Meteorological Society Section: Journal of Climate) doi: 10.1175/2008JCLI2556.1

Burchard, H. (2002). Energy-conserving discretisation of turbulent shear and buoyancy production. *Ocean Modell.*, *4*(3-4), 347–361. doi: 10.1016/S1463-5003(02)00009-4

Cohen, Y., Lopez-Gomez, I., Jaruga, A., He, J., Kaul, C. M., & Schneider, T. (2020, September). Unified Entrainment and Detrainment Closures for Extended Eddy-Diffusivity Mass-Flux Schemes. *Journal of Advances in Modeling Earth Systems*, *12*(9). Retrieved 2021-11-02, from `https://onlinelibrary.wiley.com/doi/10.1029/2020MS002162` doi: 10.1029/2020MS002162

Coppola, L., Prieur, L., Taupier-Letage, I., Estournel, C., Testor, P., Lefevre, D., ... Taillandier, V. (2017). Observation of oxygen ventilation into deep waters through targeted deployment of multiple argo-o2 floats in the northwestern mediterranean sea in 2013. *J. Geophys. Res.*, *122*(8), 6325-6341. doi: https://doi.org/10.1002/2016JC012594

Couvreux, F., Hourdin, F., & Rio, C. (2010, March). Resolved Versus Parametrized Boundary-Layer Plumes. Part I: A Parametrization-Oriented Conditional Sampling in Large-Eddy Simulations. *Boundary-Layer Meteorology*, *134*(3), 441–458. Retrieved 2022-02-21, from `https://doi.org/10.1007/s10546-009-9456-5` doi: 10.1007/s10546-009-9456-5

Couvreux, F., Hourdin, F., Williamson, D., Roehrig, R., Volodina, V., Villefranque, N., ... Xu, W. (2021). Process-Based Climate Model Development Harnessing Machine Learning: I. A Calibration Tool for Parameterization Improvement. *J. Adv. Model. Earth Syst.*, *13*(3), e2020MS002217. doi: 10.1029/2020MS002217

Cuxart, J., Bougeault, P., & Redelsperger, J.-L. (2000). A turbulence scheme allowing for mesoscale and large-eddy simulations. *Quart. J. Roy. Meteorol. Soc.*, *126*(562), 1–30. doi: 10.1002/qj.49712656202

Deardorff, J. W. (1970). Convective Velocity and Temperature Scales for the Unstable Planetary Boundary Layer and for Rayleigh Convection. *J. Atmos. Sci.*, *27*(8), 1211–1213. doi: 10.1175/1520-0469(1970)027⟨1211:CVATSF⟩2.0.CO;2

Estournel, C., Testor, P., Taupier-Letage, I., Bouin, M.-N., Coppola, L., Durand, P., ... others (2016). Hymex-sop2: The field campaign dedicated to dense water formation in the northwestern mediterranean. *Oceanography*, *29*(4), 196–206.

Garanaik, A., Pereira, F. S., Smith, K., Robey, R., Li, Q., Pearson, B., & Van Roekel, L. (2024). A New Hybrid Mass-Flux/High-Order Tur-

bulence Closure for Ocean Vertical Mixing. *Journal of Advances in Modeling Earth Systems*, *16*(1). Retrieved 2024-01-31, from https://onlinelibrary.wiley.com/doi/abs/10.1029/2023MS003846 (_eprint: https://onlinelibrary.wiley.com/doi/pdf/10.1029/2023MS003846) doi: 10.1029/2023MS003846

Garcia, J. R., & Mellado, J. P. (2014). The Two-Layer Structure of the Entrainment Zone in the Convective Boundary Layer. *J. Atmos. Sci.*, *71*(6), 1935–1955. doi: 10.1175/JAS-D-13-0148.1

Garratt, J. (1994). *The Atmospheric Boundary Layer*. Cambridge University Press.

Gaspar, P., Grégoris, Y., & Lefevre, J.-M. (1990). A simple eddy kinetic energy model for simulations of the oceanic vertical mixing: Tests at station Papa and long-term upper ocean study site. *J. Geophys. Res.*, *95*(C9), 16179–16193. doi: 10.1029/JC095iC09p16179

Giordani, H., Bourdallé-Badie, R., & Madec, G. (2020). An Eddy-Diffusivity Mass-Flux Parameterization for Modeling Oceanic Convection. *J. Adv. Model. Earth Syst.*, *12*. doi: 10.1029/2020MS002078

Haghshenas, A., & Mellado, J. P. (2019a). Characterization of wind-shear effects on entrainment in a convective boundary layer. *J. Fluid Mech.*, *858*, 145–183. doi: 10.1017/jfm.2018.761

Haghshenas, A., & Mellado, J. P. (2019b, January). Characterization of wind-shear effects on entrainment in a convective boundary layer. *J. Fluid Mech.*, *858*, 145–183. Retrieved 2023-10-11, from https://www.cambridge.org/core/product/identifier/S0022112018007619/type/journal_article doi: 10.1017/jfm.2018.761

Han, J., & Bretherton, C. S. (2019). TKE-Based Moist Eddy-Diffusivity Mass-Flux (EDMF) Parameterization for Vertical Turbulent Mixing. *Weather Forecast.*, *34*(4), 869–886. doi: 10.1175/WAF-D-18-0146.1

Honnert, R. (2022). *De la zone grise de la turbulence à AROME hectométrique* (thesis, Université Toulouse 3 Paul Sabatier). Retrieved from https://hal.science/tel-03600147

Houpert, L., Durrieu de Madron, X., Testor, P., Bosse, A., D'Ortenzio, F., Bouin, M. N., ... Raimbault, P. (2016). Observations of open-ocean deep convection in the northwestern mediterranean sea: Seasonal and interannual variability of mixing and deep water masses for the 2007-2013 period. *J. Geophys. Res.*, *121*(11), 8139-8171. Retrieved from https://agupubs.onlinelibrary.wiley.com/doi/abs/10.1002/2016JC011857 doi: https://doi.org/10.1002/2016JC011857

Hourdin, F., Mauritsen, T., Gettelman, A., Golaz, J.-C., Balaji, V., Duan, Q., ... Williamson, D. (2017). The Art and Science of Climate Model Tuning. *Bull. Amer. Meteor. Soc.*, *98*(3), 589–602. doi: 10.1175/BAMS-D-15-00135.1

Lac, C., Chaboureau, J.-P., Masson, V., Pinty, J.-P., Tulet, P., Escobar, J., ... Wautelet, P. (2018). Overview of the Meso-NH model version 5.4 and its applications. *Geosci. Model Dev.*, *11*(5), 1929–1969. doi: 10.5194/gmd-11-1929-2018

Legay, A., Deremble, B., Penduff, T., Brasseur, P., & Molines, J.-M. (2023). *A generic framework for evaluating the oceanic mixed layer depth dynamics* (preprint). Preprints. doi: 10.22541/essoar.168563421.17506622/v1

Madec, G., Bourdallé-Badie, R., Chanut, J., Clementi, E., Coward, A., Ethé, C., ... Samson, G. (2019). *NEMO ocean engine*. Retrieved from https://zenodo.org/record/1464816 doi: 10.5281/ZENODO.1464816

Marshall, J., & Schott, F. (1999). Open-ocean convection: Observations, theory, and models. *Rev. Geophys.*, *37*(1), 1–64. doi: 10.1029/98RG02739

McDougall, T. J. (2003). Potential Enthalpy: A Conservative Oceanic Variable for Evaluating Heat Content and Heat Fluxes. *J. Phys. Oceanogr.*, *33*(5), 945–963. doi: 10.1175/1520-0485(2003)033⟨0945:PEACOV⟩2.0.CO;2

Mellor, G. (1973). Analytic Prediction of the Properties of Stratified Planetary Surface Layers. *J. Atmos. Sci.*, *30*(6), 1061–1069. doi: 10.1175/1520-0469(1973)030⟨1061:APOTPO⟩2.0.CO;2

Obukhov, A. M. (1971). Turbulence in an atmosphere with a non-uniform temperature. *Bound.-Lay. Meteorol.*, *2*(1), 7–29. doi: 10.1007/BF00718085

Pergaud, J., Masson, V., Malardel, S., & Couvreux, F. (2009). A Parameterization of Dry Thermals and Shallow Cumuli for Mesoscale Numerical Weather Prediction. *Bound.-Lay. Meteorol.*, *132*, 83–106. doi: 10.1007/s10546-009-9388-0

Perrot, M., Lemarié, F., & Dubos, T. (2024, February). *Energetically consistent Eddy-Diffusivity Mass-Flux schemes. part i: Theory and models.* Retrieved from `https://hal.science/hal-04439113`

Peterson, P. (2009). F2PY: a tool for connecting Fortran and Python programs. *Int. j. comput. sci. eng.*, *4*(4), 296. doi: 10.1504/IJCSE.2009.029165

Pope, S. B. (2004). Ten questions concerning the large-eddy simulation of turbulent flows. *New J. Phys.*, *6*, 35–35. doi: 10.1088/1367-2630/6/1/035

Ramadhan, A., Wagner, G. L., Hill, C., Campin, J.-M., Churavy, V., Besard, T., ... Marshall, J. (2020). Oceananigans.jl: Fast and friendly geophysical fluid dynamics on GPUs. *Journal of Open Source Software*, *5*(53), 2018. Retrieved from `https://doi.org/10.21105/joss.02018` doi: 10.21105/joss.02018

Rio, C., Hourdin, F., Couvreux, F., & Jam, A. (2010). Resolved Versus Parametrized Boundary-Layer Plumes. Part II: Continuous Formulations of Mixing Rates for Mass-Flux Schemes. *Bound.-Lay. Meteorol.*, *135*(3), 469–483. doi: 10.1007/s10546-010-9478-z

Siebesma, A. P., Soares, P. M. M., & Teixeira, J. (2007). A Combined Eddy-Diffusivity Mass-Flux Approach for the Convective Boundary Layer. *J. Atmos. Sci.*, *64*(4), 1230–1248. doi: 10.1175/JAS3888.1

Soares, P. M. M., Miranda, P. M. A., Siebesma, A. P., & Teixeira, J. (2004). An eddy-diffusivity/mass-flux parametrization for dry and shallow cumulus convection. *Quart. J. Roy. Meteorol. Soc.*, *130*(604), 3365–3383. doi: 10.1256/qj.03.223

Souza, A. N., Wagner, G. L., Ramadhan, A., Allen, B., Churavy, V., Schloss, J., ... Ferrari, R. (2020). Uncertainty Quantification of Ocean Parameterizations: Application to the K-Profile-Parameterization for Penetrative Convection. *J. Adv. Model. Earth Syst.*, *12*(12). doi: 10.1029/2020MS002108

Tailleux, R., & Dubos, T. (2024, April). A simple and transparent method for improving the energetics and thermodynamics of seawater approximations: Static energy asymptotics (SEA). *Ocean Modelling*, *188*, 102339. Retrieved 2024-05-07, from `https://www.sciencedirect.com/science/article/pii/S146350032400026X` doi: 10.1016/j.ocemod.2024.102339

Tan, Z., Kaul, C. M., Pressel, K. G., Cohen, Y., Schneider, T., & Teixeira, J. (2018). An Extended Eddy-Diffusivity Mass-Flux Scheme for Unified Representation of Subgrid-Scale Turbulence and Convection. *J. Adv. Model. Earth Syst.*, *10*(3), 770–800. doi: 10.1002/2017MS001162

Turner, J. S. (1979). *Buoyancy Effects in Fluids.* Cambridge University Press.

Van Roekel, L., Adcroft, A. J., Danabasoglu, G., Griffies, S. M., Kauffman, B., Large, W., ... Schmidt, M. (2018). The KPP Boundary Layer Scheme for the Ocean: Revisiting Its Formulation and Benchmarking One-Dimensional Simulations Relative to LES. *J. Adv. Model. Earth Syst.*, *10*(11), 2647–2685. doi: 10.1029/2018MS001336

Waldman, R., Somot, S., Herrmann, M., Bosse, A., Caniaux, G., Estournel, C., ... Testor, P. (2017). Modeling the intense 2012-2013 dense water formation event in the northwestern mediterranean sea: Evaluation with an ensemble simulation approach. *J. Geophys. Res.*, *122*(2), 1297-1324. doi: https://doi.org/10.1002/2016JC012437

Witek, M. L., Teixeira, J., & Matheou, G. (2011). An Eddy Diffusivity–Mass

Flux Approach to the Vertical Transport of Turbulent Kinetic Energy in Convective Boundary Layers. *J. Atmos. Sci.*, *68*(10), 2385–2394. doi: 10.1175/JAS-D-11-06.1

Yano, J.-I. (2014). Formulation structure of the mass-flux convection parameterization. *Dynam. Atmos. Oceans*, *67*, 1–28. doi: 10.1016/j.dynatmoce.2014.04.002

Zheng, Z., Harcourt, R. R., & D'Asaro, E. A. (2021). Evaluating Monin–Obukhov Scaling in the Unstable Oceanic Surface Layer. *J. Phys. Oceanogr.*, *51*(3), 911–930. doi: 10.1175/JPO-D-20-0201.1